Wγ production in hadronic collisions using the POWHEG+MiNLO method

Luca Barzè,[a] **Mauro Chiesa,**[b,d] **Guido Montagna,**[b,d] **Paolo Nason,**[c] **Oreste Nicrosini,**[d] **Fulvio Piccinini**[d] **and Valeria Prosperi**[b,d]

[a]*PH-TH Department, CERN,*
  Geneva, CH-1211 Switzerland

[b]*Dipartimento di Fisica, Università di Pavia,*
  Via A. Bassi 6, Pavia, 27100 Italy

[c]*INFN, Sezione di Milano Bicocca,*
  Piazza della Scienza 3, Milano, 20126 Italy

[d]*INFN, Sezione di Pavia,*
  Via A. Bassi 6, Pavia, 27100 Italy

 E-mail: luca.barze@cern.ch, mauro.chiesa@pv.infn.it,
 guido.montagna@pv.infn.it, paolo.nason@mib.infn.it,
 oreste.nicrosini@pv.infn.it, fulvio.piccinini@pv.infn.it,
 valeria.prosperi@pv.infn.it

ABSTRACT: We detail a calculation of $W\gamma$ production in hadronic collision, at Next-to-Leading Order (NLO) QCD interfaced to a shower generator according to the POWHEG prescription supplemented with the MiNLO procedure. The fixed order result is matched to an interleaved QCD+QED parton shower, in such a way that the contribution arising from hadron fragmentation into photons is fully modeled. In general, our calculation illustrates a new approach to the fully exclusive simulation of prompt photon production processes accurate at the NLO level in QCD. We compare our predictions to those of the NLO program MCFM, which treats the fragmentation contribution in terms of a photon fragmentation functions. We also perform comparisons to available LHC data at 7 TeV, for which we observe good agreement, and provide phenomenological results for physics studies of the $W\gamma$ production process at the Run II of the LHC. The new tool, which includes W leptonic decays and the contribution of anomalous gauge couplings, allows a fully exclusive, hadron-level description of the $W\gamma$ process, and is publicly available at the repository of the POWHEG BOX. Our approach can be easily adapted to deal with other relevant isolated photon production processes in hadronic collisions.

Contents

1   Introduction

With the discovery of a new scalar particle in the search for the Standard Model (SM) Higgs boson by the ATLAS [1] and CMS [2] collaborations at the Large Hadron Collider (LHC), all the particles postulated by the SM have been identified. In parallel to the present efforts which are mainly focused on studying the properties of the newly discovered boson, other important studies set the physics agenda of the LHC, ranging from measurements of SM processes to the search for new phenomena.

In this general context, diboson production processes play a particularly interesting rôle for different reasons [3]. They represent the primary backgrounds to Higgs and new physics searches, and provide direct information on the self-interactions of the electroweak (EW) gauge bosons. Since the form and strength of the non-abelian gauge couplings are fixed by the underlying $\text{SU}(2) \otimes \text{U}(1)$ symmetry, any deviation of these couplings from their SM values would be indicative of new physics.

Aside from $\gamma\gamma$ production, the production processes of a W or Z boson in association with an isolated photon provide the largest and cleanest yields among diboson final states

at hadron colliders, as backgrounds to $W\gamma$ and $Z\gamma$ production can be significantly reduced through the identification of the W and Z bosons via their leptonic decay modes. Measurements of $V\gamma$ ($V = W, Z$) processes from initial analyses at the LHC have been performed both by the ATLAS [4–7] and by the CMS collaboration [8–10]. These measurements have been used to test the SM predictions, to set limits on anomalous triple gauge couplings (ATGCs) and on the production of new vector resonances. Previous measurements of $V\gamma$ final states in hadronic collisions have been made at the Tevatron by the CDF [11] and D0 [12, 13] collaborations and used to set limits on ATGCs, that are improved by the current analyses at the LHC. Constraints from LEP on ATGCs are summarized in ref. [14].

At the LHC, the signal events $pp \rightarrow \ell\nu\gamma + X, \ell = e, \mu$ (for $W\gamma$ production) and $pp \rightarrow \ell^+\ell^-\gamma + X, \nu\bar{\nu}\gamma + X$ (for $Z\gamma$ production) are modeled in the latest analyses using the leading-order (LO) matrix element generators ALPGEN [15], MADGRAPH [16] and SHERPA [17]. Broadly speaking, the above LO predictions are found to reproduce the shape of the photon distributions and the kinematic properties of the leptons and jets in $V\gamma$ candidate events. Afterwards, the cross section measurements are compared to the Next-to-Leading Order (NLO) QCD predictions of the parton-level Monte Carlo (MC) program MCFM [18], that includes the full set of LO diagrams and NLO QCD corrections contributing to $V\gamma$ production, and takes care of the contribution coming from the fragmentation of secondary quarks and gluons into isolated photons via the formalism of (collinear) photon fragmentation functions [19]. The effects of ATGCs can be simulated in MCFM as well.[1] Limits on ATGCs are set by ATLAS using MCFM and by CMS using SHERPA.

The state of the art of the theoretical tools used in the experimental analyses of $V\gamma$ processes at the LHC points out clearly that progress in this area would be welcome. In fact, it is known that LO matrix element generators matched to Parton Showers (PS) provide a reliable description of the shape of the differential cross sections of experimental interest (even in the presence of a high jet multiplicity) but can not predict their normalization with the desired accuracy. On the other hand, the results of NLO parton-level programs must be corrected to compare the predictions to the measured cross sections. Moreover, the lack of higher-order QCD contributions in fixed-order MCs can give rise to biases in the predicted cross sections, especially for those observables significantly affected by the contribution of multiple QCD radiation. In particular, in view of the next data taking at the LHC at higher energy and higher luminosity, the improvement of the accuracy of the theoretical predictions is becoming a pressing issue, as the experimental errors of the measurements will diminish and work will continue towards highlighting deviations, if any, from the apparent SM behaviour.

Given the above motivations, the main aim of the present work is to provide a new simulation tool for the study of $W\gamma$ production at the LHC. By doing so, we also detail

---

[1] Previous calculations of NLO QCD corrections to $V\gamma$ production in hadronic collisions can be found in refs. [20–23]. NNLO QCD corrections to $Z\gamma$ production have been computed in ref. [24], while recent progress in the calculation of NNLO QCD corrections to the $W\gamma$ process is documented in ref. [25]. NLO QCD corrections to the related processes $W\gamma$ and $Z\gamma$ plus one or two jets have been calculated in ref. [26] and refs. [27–29], respectively. NLO EW corrections, not considered in the present study, to $W\gamma$ and $Z\gamma$ production at the LHC have been computed in the leading-pole approximation in ref. [30] and to $Z\gamma$ production exactly in ref. [31].

a new exclusive MC approach to the simulation of prompt-photon production in hadronic collisions, which includes a number of novel features with respect to previous methods proposed in the literature.

Our generator is built according to the POWHEG method [32, 33], within the POWHEG BOX framework [34], that allows to interface an NLO calculation to a PS generator. We propose a description of the process and, in particular, of the fragmentation mechanism which includes the contribution of higher-order matrix elements interfaced to a mixed QCD+QED PS. For the treatment of the matrix elements that are not integrable over the full phase space, as well as to ensure sensible results and a smooth behaviour near the Sudakov regions, we use the MiNLO (Multi-scale improved NLO) method developed in refs. [35, 36]. We also include the contribution of ATGCs according to the standard CP-conserving Lagrangian parameterization adopted in the experimental analyses.

The work presented here is the first NLOPS (NLO calculation interfaced to a PS) simulation of $W\gamma$ production in hadronic collisions. Its theoretical framework is novel, and can be applied to other processes involving the production of isolated photons. The relative computer code is made available in the public repository of the POWHEG BOX [34] at the web site http://powhegbox.mib.infn.it.

The basic idea underlying our method is to treat electromagnetic and strong radiation on the same footing within the POWHEG approach. Given the basic process of $q\bar{q}' \to W\gamma$ production, POWHEG generates the strong radiation using the real matrix elements for the process $jj \to W\gamma j$, where j stands here for any parton.[2] POWHEG will separate the real cross section into a sum of different contributions, corresponding to the singular regions of the real amplitude. If electromagnetic and strong radiation are treated on the same footing, there will be two kinds of singular regions: those where the emitted parton j is the collinear one, and those where the photon is collinear (either to the initial state partons, or to the electron coming from the decay of the W). The two different kinds of regions will have two different kinds of underlying Born processes,[3] the $q\bar{q}' \to W\gamma$ ones and a $jj \to Wj$ ones. Thus, in this approach we are forced, for consistency, to introduce also the $jj \to Wj$ process as a possible Born process. According to the POWHEG formalism, a $jj \to Wj$ initial process may radiate a gluon or a photon, according to competing QED and QCD Sudakov form factor, with the gluon radiation being favoured. In case a photon is generated, the event will be passed to a shower generator, that will not be allowed to produce splittings that are harder than the radiated photon. The corresponding event will typically have a hard jet, a less hard photon, and more partons, limited in hardness by the photon hardness. In the more likely case that a coloured parton is generated, the event will be passed to a shower, that will not be allowed to produce splittings that are harder than the POWHEG radiated parton. If the PS generator includes QED radiation, hard photons may also be produced by the shower. It is clear that in this approach the full photon radiation phase space will be reconstructed from different components:

- The $q\bar{q}' \to W\gamma$ initiated event, where the hardest radiation is a photon radiation.

---

[2]Here and in the following, when we indicate a final state W we imply that we are considering its leptonic decay.

[3]The underlying Born process for a given singular region is obtained by merging the collinear particles relative to a given singular region.

- The $jj \to Wj$ initiated event followed by photon radiation from POWHEG, where the hardest radiation is a coloured parton, and the second hardest is a photon.

- The $jj \to Wj$ initiated event followed by parton radiation from POWHEG, where the hardest radiation is a coloured parton, the second hardest is also a coloured parton, and where a photon may still be generated by the shower as the third, or fourth and so on, hardest radiation.

Notice that within this approach the direct and fragmentation production mechanisms are treated in a seamless way. Most photon radiation is treated perturbatively, either with the LO and NLO matrix elements in POWHEG, or in the PS within the collinear approximation. Ultimately, the hadronization step may also lead to photons, and whether or not this transition is treated correctly will depend upon the degree of accuracy of the shower MC generator.

All major general purpose PS generators implement interleaved QCD and QED radiation, thus they model associated photon production from a given hard process in the collinear approximation (see ref. [37] and references therein). An improved approach based upon the usage of LO multiparton matrix elements and an interleaved QCD+QED PS can be found in ref. [38], where results for the inclusive production of isolated photons and diphoton production are given in comparison to Tevatron measurements. In this approach also large angle photon and parton emission, as well as their interplay, is described with LO matrix elements accuracy.

A first attempt to simulate photon production processes in hadronic collisions at NLOPS accuracy according to the POWHEG method has been developed in ref. [39] and applied to diphoton production. We will discuss and clarify similarities and differences of this method with respect to our schemes, by also providing an optional variant of our generator that mimics it closely.

A completely different approach to prompt photon production, applied to the $t\bar{t}\gamma$ and $t\bar{t}\gamma\gamma$ production processes, has appeared recently in refs. [40, 41]. We will further comment about this approach in the Conclusions.

The paper is organized as follows. In section 2 we describe the theoretical details of our approach, paying particular attention to the method used for the generation of the hardest emission and for the treatment of the photon fragmentation process, which is one of the main issues of the calculation. In section 3 we illustrate comparisons of our predictions to MCFM calculations and to LHC data at $7\,\mathrm{TeV}$, and we show a sample of numerical results for physics studies at the LHC at $14\,\mathrm{TeV}$. We present our conclusions in section 4.

2 Theoretical framework

2.1 Leading order contributions and anomalous couplings

At LO, the production of a W boson and a photon in hadronic collisions, with leptonic decays of the vector boson, is an EW process which proceeds via quark-antiquark annihilation

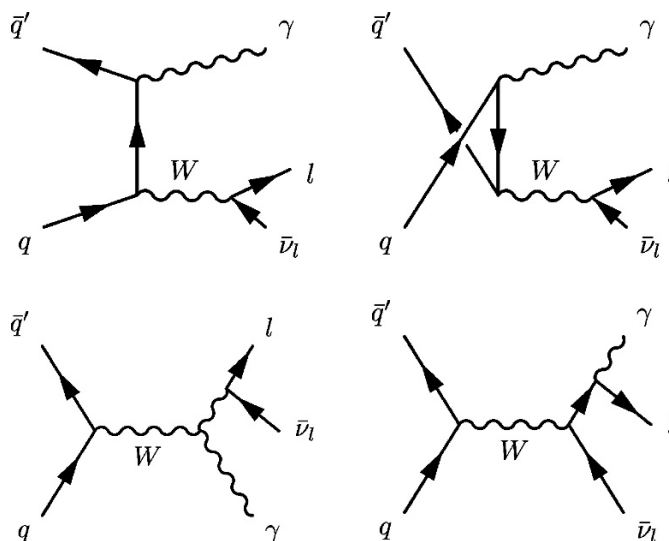$$q\bar{q}' \to \ell^{\pm}\nu\gamma, \qquad \ell = e, \mu \tag{2.1}$$

Figure 1. LO Feynman diagrams for the $\ell\nu\gamma$ production process in hadronic collisions.

in terms of the Feynman diagrams shown in figure 1. The first three diagrams are typically classified as direct photon radiation in the production process, while the last diagram corresponds to final-state photon emission from the lepton in the W decay. We computed the corresponding LO amplitude, which retains full spin correlations in the decay and interference effects, by using the computer algebra program FORM [42]. A prominent feature of the $W\gamma$ LO matrix element is the appearance of a so called radiation zero, which corresponds to the existence of some kinematic configurations for which the amplitude vanishes [43, 44]. This can appear in some observables as dip in the rapidity distributions and can provide a handle to extract information on the anomalous couplings, since the latter partially fill the dip. It is known that NLO QCD corrections modify the LO results by partially filling the gap [21]. Fortunately, the sensitivity to the ATGCs can be largely recovered by imposing a jet veto [23]. Interestingly, an analysis of this kind has been recently made by the CMS collaboration [8] by measuring the differential yield as a function of the charge-signed rapidity difference between a photon candidate and a lepton in $W\gamma$ candidates.[4] The distributions measured at the LHC clearly demonstrate the characteristic radiation zero expected for $W\gamma$ production, in agreement with the SM prediction.

The $WW\gamma$ vertex relevant for the limits on ATGCs enters via the third diagram in figure 1. In our calculation, we included the contribution of ATGCs according to the parameterization used at the LHC and in previous measurements at hadron and e^+e^- colliders. We introduced the anomalous contributions to the $WW\gamma$ vertex in terms of the Feynman rules associated to the following effective Lagrangian [46–50]

$$\mathcal{L}_{WW\gamma} = -ie\left[\left(W_{\mu\nu}^\dagger W^\mu A^\nu - W_\mu^\dagger A_\nu W^{\mu\nu}\right) + k_\gamma W_\mu^\dagger W_\nu F^{\mu\nu} + \frac{\lambda_\gamma}{M_W^2} W_{\lambda\mu}^\dagger W_\nu^\mu F^{\nu\lambda}\right] . \quad (2.2)$$

---

[4]A first study of the radiation-amplitude zero in $W\gamma$ production using such an observable was made by the D0 collaboration in proton-antiproton collisions at the Tevatron [45].
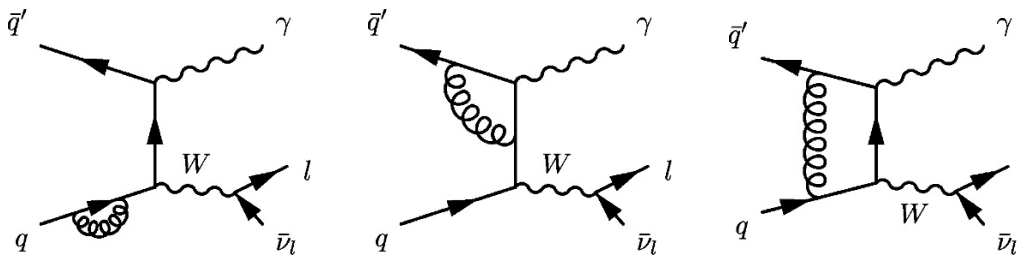
Figure 2. Sample graphs for the virtual QCD corrections to $q\bar{q}' \to \ell\nu\gamma$ production.

In eq. (2.2) A^μ and W^μ are the photon and W^- field, respectively, $W_{\mu\nu} = \partial_\mu W_\nu - \partial_\nu W_\mu$, $F_{\mu\nu} = \partial_\mu A_\nu - \partial_\nu A_\mu$, e is the positron charge and M_W represents the W mass. The effective Lagrangian of eq. (2.2) satisfies electromagnetic gauge invariance, as well as C and P invariance. In the SM $k_\gamma = 1$ and $\lambda_\gamma = 0$. The effect of ATGCs is expressed in terms of their deviation from the SM values, leading to the two parameter set $(\lambda_\gamma, \Delta k_\gamma)$, with $\Delta k_\gamma \equiv k_\gamma - 1$.[5] The full amplitude resulting from the calculation of the diagrams shown in figure 1 with the modifications introduced by the Lagrangian of eq. (2.2) has been computed using FORM.

As a cross-check, we compared our LO predictions, both without and with ATGCs, with those of MCFM, finding perfect agreement.

2.2 NLO QCD corrections

The NLO QCD corrections to $W\gamma$ production can be obtained by dressing the diagrams of figure 1 with both virtual and real gluon radiation.

The virtual corrections due to the interference of one-loop diagrams with the Born amplitude comprise self-energy, vertex and box corrections to the quark lines of figure 1. Sample graphs for the virtual corrections to the t-channel $q\bar{q}' \to W\gamma$ topology are shown in figure 2.

Consistently with the POWHEG method and the POWHEG BOX requirements, we computed the finite part of the virtual cross section in conventional dimensional regularization, using the Passarino-Veltman tensor reduction [52]. In order to compare with the predictions of MCFM, where the NLO calculation is performed in the dimensional reduction scheme, we translated our result for the virtual contribution from dimensional regularization to dimensional reduction, according to the rule given in ref. [34] (see also ref. [53]). We checked that the results of MCFM and those of our calculation perfectly agree. However, because the calculation of the one-loop corrections using the MCFM matrix elements is less CPU demanding, we included them in our implementation.

The real radiation contributions are obtained by attaching a gluon to the LO diagrams of figure 1 in all possible ways. The contributions with one extra parton in the final state

---

[5]The theoretical and phenomenological drawbacks of the anomalous coupling approach in favor of the virtues of a modern effective field theory approach have been recently discussed in ref. [51]. However, as shown in ref. [51], the results obtained using the anomalous coupling formalism can be reframed in terms of the effective field theory framework, if only dimension-six operators are considered and the anomalous couplings are treated as constants, i.e. independent of energy.
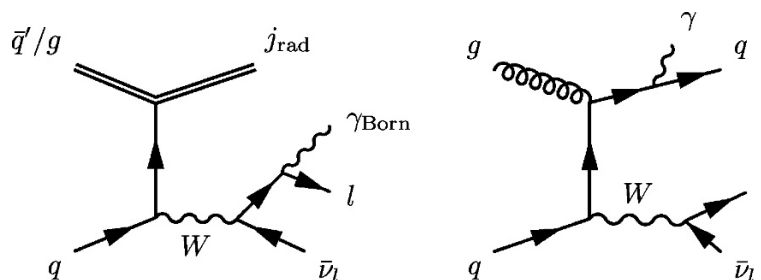
Figure 3. Sample graphs for real radiation contributions to $q\bar{q}' \to \ell\nu\gamma$ production. Left diagram: QCD radiation in $\ell\nu\gamma$ production with photon emission from the final-state lepton; right diagram: gluon-induced process with photon emission from a final-state parton, associated to a fragmentation contribution.

are the $2 \to 4$ processes $q\bar{q}' \to \ell\nu\gamma g$ and $gq/\bar{q}' \to \ell\nu\gamma\bar{q}'/q$. Two examples of Feynman diagrams for real radiation contributions to $W\gamma$ production are shown in figure 3.

We computed the real radiation Feynman diagrams using `FORM`. Also in this case, we compared our calculation with `MCFM`, finding perfect agreement. We implemented in the `POWHEG BOX` the real radiation matrix elements extracted from `MCFM`, as the latter ensure the best CPU performances by virtue of the helicity formalism used there.[6]

The real radiation processes contain QCD singularities due to collinear gluon emission, as well as QED singularities corresponding to configurations where a parton becomes collinear to a photon, which do not cancel when summing up the real and virtual QCD pieces. In the following we will come back to the treatment of this aspect in our approach. For the moment, let us remind that in NLO QCD calculations of $V\gamma$ [21–23] and other isolated photon production processes [54–56] at hadron colliders, as well as in fixed-order MC programs for prompt-photon in hadronic collisions, like e.g. `MCFM`, `DIPHOX` [57] and `JETPHOX` [58, 59], the QED divergences associated to a final-state parton becoming collinear to a photon are treated in terms of (non-perturbative) quark/gluon fragmentation functions into photons $D_a^\gamma(z, \mu^2), a = q, g$. They describe the probability of finding a photon with longitudinal momentum fraction z in a quark or gluon jet at a given fragmentation scale μ [60, 61]. Since the photon fragmentation functions are of the (leading) order $\alpha_{\rm em}/\alpha_{\rm S}$, the fragmentation contribution[7] is of the same order as LO direct production, and at high-energy hadron colliders can become a relevant source of prompt photon production because of the large impact of the gluon distribution function. However, its magnitude strongly depends on the applied experimental cuts and can be drastically reduced by imposing appropriate isolation criteria. Among the different criteria for the isolation of photons there are: the cone approach [62, 63], the democratic approach [64] and the smooth isolation prescription [65]. In particular, according to the latter algorithm, the contribution of the fragmentation mechanism is eliminated by a prescription which is IR safe at all orders, and the isolated-photon cross section depends on the direct production

---

[6]Note that in the computation of the all real radiation processes yielding the signature $\ell\nu\gamma+j$, $j = q, \bar{q}', g$ we included the contribution of ATGCs as well, in order to ensure infrared (IR) cancellation between virtual and real corrections in the presence of anomalous couplings.

[7]This contribution is also known in the literature as "bremsstrahlung".

process only.[8] The smooth isolation prescription is widely applied in perturbative QCD calculations but its implementation is very cumbersome from the experimental point of view since it requires ideal detectors with very fine granularity.

The QCD infrared singularities present at intermediate steps of the calculation in the real emission and virtual contributions have been treated using the FKS subtraction formalism [66] provided by the POWHEG BOX. To regulate the singularities due to photon emission in gluon-induced real radiation processes we used the expressions of the QED counterterms and collinear remnants introduced in refs. [67, 68] for the implementation of the EW corrections to single vector boson production in the POWHEG BOX.

2.3 Details of the POWHEG implementation

In this section, we describe our method for the treatment of the $W(\to \ell\nu)\gamma$ process. In the following, for brevity, we will sometimes omit to indicate the W decay product when referring to a process. The reader should remember that the decay process is always implied.

2.3.1 The POWHEG method

To illustrate our approach, it is first necessary to remind the master formula and the algorithm used in POWHEG for the cross section calculation and event generation. It is given by (in the standard POWHEG notation) [33]

$$
d\sigma = \sum_{f_b} \bar{B}^{f_b}(\mathbf{\Phi}_{\mathrm{B}}) \, d\mathbf{\Phi}_{\mathrm{B}} \left\{ \Delta^{f_b}(\mathbf{\Phi}_{\mathrm{B}}, p_{\mathrm{T}}^{\min}) \right.
$$
$$
\left. + \sum_{\alpha_{\mathrm{r}} \in \{\alpha_{\mathrm{r}}|f_b\}} \frac{\left[d\mathbf{\Phi}_{\mathrm{rad}} \, \theta\left(k_{\mathrm{T}} - p_{\mathrm{T}}^{\min}\right) \Delta^{f_b}(\mathbf{\Phi}_{\mathrm{B}}, k_{\mathrm{T}}) \, R\left(\mathbf{\Phi}_{n+1}\right) \right]_{\alpha_{\mathrm{r}}}^{\bar{\mathbf{\Phi}}_n^{\alpha_{\mathrm{r}}} = \mathbf{\Phi}_{\mathrm{B}}}}{B^{f_b}(\mathbf{\Phi}_{\mathrm{B}})} \right\}. \quad (2.3)
$$

For each contributing flavor structure f_b to a given n-body process, the two basic ingredients of eq. (2.3) are the NLO inclusive cross section $\bar{B}^{f_b}(\mathbf{\Phi}_{\mathrm{B}})$ and the (modified) Sudakov form factor $\Delta^{f_b}(\mathbf{\Phi}_{\mathrm{B}}, p_{\mathrm{T}})$ for the calculation of the emission probability. According to the POWHEG method, the n-body configuration is generated according to $\bar{B}^{f_b}(\mathbf{\Phi}_{\mathrm{B}})$ and the hardest emission is generated using the Sudakov form factor $\Delta^{f_b}(\mathbf{\Phi}_{\mathrm{B}}, p_{\mathrm{T}})$. Then the events can be showered by a PS algorithm ordered in transverse momentum.

The $\bar{B}^{f_b}(\mathbf{\Phi}_{\mathrm{B}})$ cross section at NLO accuracy can be written as

$$
\bar{B}^{f_b}(\mathbf{\Phi}_{\mathrm{B}}) = \left[B\left(\mathbf{\Phi}_{\mathrm{B}}\right) + V\left(\mathbf{\Phi}_{\mathrm{B}}\right) \right]_{f_b} + \sum_{\alpha_{\mathrm{r}} \in \{\alpha_{\mathrm{r}}|f_b\}} \int \left[d\mathbf{\Phi}_{\mathrm{rad}} \left\{ R\left(\mathbf{\Phi}_{n+1}\right) - C\left(\mathbf{\Phi}_{n+1}\right) \right\} \right]_{\alpha_{\mathrm{r}}}^{\bar{\mathbf{\Phi}}_n^{\alpha_{\mathrm{r}}} = \mathbf{\Phi}_{\mathrm{B}}}
$$
$$
+ \sum_{\alpha_{\oplus} \in \{\alpha_{\oplus}|f_b\}} \int \frac{dz}{z} \, G_{\oplus}^{\alpha_{\oplus}}(\mathbf{\Phi}_{n,\oplus}) + \sum_{\alpha_{\ominus} \in \{\alpha_{\ominus}|f_b\}} \int \frac{dz}{z} \, G_{\ominus}^{\alpha_{\ominus}}(\mathbf{\Phi}_{n,\ominus}). \quad (2.4)
$$

---

[8]It is worth mentioning that a further source of final-state photons comes from the decays of mesons, such as π^0, η or ω. However, such a mechanism, which is much larger than prompt-photon production, constitutes a background to high p_{T} photon production and experimental measurements are corrected for this effect.

In eq. (2.4) $B\left(\boldsymbol{\Phi}_{\mathrm{B}}\right)$ is the LO cross section at fixed underlying Born flavour f_b and kinematics $\boldsymbol{\Phi}_{\mathrm{B}}$, the real contribution $R\left(\boldsymbol{\Phi}_{n+1}\right)$ is the squared matrix element describing the radiation of an extra parton over the radiative phase-space variables $d\Phi_{\mathrm{rad}}$, which is regulated by subtracting the counterterms $C\left(\boldsymbol{\Phi}_{n+1}\right)$ containing the same singularities as $R\left(\boldsymbol{\Phi}_{n+1}\right)$. The finite contribution $V\left(\boldsymbol{\Phi}_{\mathrm{B}}\right)$ includes the virtual loop corrections and the counterterms integrated over the real emission variables, which cancel the singularities from the loop corrections. The factors $G_{\oplus}^{\alpha_{\oplus}}\left(\boldsymbol{\Phi}_{n,\oplus}\right)$ and $G_{\ominus}^{\alpha_{\ominus}}\left(\boldsymbol{\Phi}_{n,\ominus}\right)$ are the collinear remnants, that are the finite leftover of the subtraction procedure that is applied to absorb the initial-state collinear singularities into the parton distribution functions (PDFs).

In the `POWHEG` algorithm, the real contributions are separated into singular contributions, corresponding to soft and collinear emission, labelled by the index α_{r}. Each α_{r} denotes a single flavour structure, and a single singular region. Each term $R_{\alpha_{\mathrm{r}}}$ is singular only in the singular region denoted by α_{r}. In eq. (2.3) and eq. (2.4), the notation $\alpha_{\mathrm{r}} \in \{\alpha_{\mathrm{r}}|f_b\}$ means all the real singular contributions that have f_b as underlying Born flavor. The square brackets with subscript α_{r} and superscript $\bar{\boldsymbol{\Phi}}_n^{\alpha_{\mathrm{r}}} = \boldsymbol{\Phi}_{\mathrm{B}}$ mean that everything inside refers to the particular real contribution labelled by α_{r}, and having underlying Born kinematics equal to $\boldsymbol{\Phi}_{\mathrm{B}}$.

In place of the standard definition of Sudakov form factor based on the usage of collinear splitting functions, the modified Sudakov form factor used in `POWHEG` is defined in terms of the real radiation matrix element as follows

$$
\Delta^{f_b}(\boldsymbol{\Phi}_{\mathrm{B}}, p_{\mathrm{T}}) = \exp\left\{ -\sum_{\alpha_{\mathrm{r}} \in \{\alpha_{\mathrm{r}}|f_b\}} \int \frac{\left[d\Phi_{\mathrm{rad}}\, R\left(\boldsymbol{\Phi}_{n+1}\right)\, \theta\left(k_{\mathrm{T}}(\boldsymbol{\Phi}_{n+1}) - p_{\mathrm{T}}\right)\right]_{\alpha_{\mathrm{r}}}^{\bar{\boldsymbol{\Phi}}_n^{\alpha_{\mathrm{r}}} = \boldsymbol{\Phi}_{\mathrm{B}}}}{B^{f_b}\left(\boldsymbol{\Phi}_{\mathrm{B}}\right)} \right\},
$$
(2.5)

where $k_{\mathrm{T}}(\boldsymbol{\Phi}_{n+1})$ is a function of the real phase space that coincides with the transverse momentum of the emitted parton in the soft and collinear limit. Given an underlying Born flavour and kinematics configuration f_b, $\boldsymbol{\Phi}_{\mathrm{B}}$, `POWHEG` generates the first, hardest emission with a probability distribution equal to the full differential of the Sudakov form factor. In particular, the transverse momentum of the hardest radiation is generated with a probabilty distribution proportional to $\mathrm{d}\Delta^{f_b}(\boldsymbol{\Phi}_{\mathrm{B}}, p_{\mathrm{T}})$. This is achieved in practice, by writing the Sudakov form factor of eq. (2.5) as a product of individual Sudakov form factors associated with each α_{r}, generating one p_{T} value for each one of them, and picking the largest one, according to the so called "highest bid method". Thus, the α_{r} regions compete among each other for the generation of radiation. Following the hardest radiation, subsequent radiations are simulated via a PS, with the restriction that radiation harder than the `POWHEG` generated one is vetoed.

2.3.2   Treatment of the direct photon and photon fragmentation contribution

Here we detail how the various components of our calculation have been included in the `POWHEG BOX`, and how the `POWHEG` method has been adapted to deal with the direct photon and photon fragmentation contributions.

We realized two implementations of the $W\gamma$ process, that differ in the treatment of radiation for events with Wj underlying Born. We label them as NC (that stands for "*with no competition*") and C ("*with competition*"), since the difference is related to whether or not in the generation of radiation in events with Wj underlying Born, the parton emission competes with photon emission, as we will clarify in the following. The NC implementation uses a method very similar to the one proposed by D'Errico and Richardson in ref. [39], and we include it to make contact with the approach proposed there, and to clarify the differences with the C implementation, that is the one that we advocate.

In both the NC and C scheme, the Born subprocesses are those for $q\bar{q}' \to \ell\nu\gamma$ and the $q\bar{q}' \to \ell\nu g$ subprocess with its crossings, corresponding to an incoming gluon and quark or antiquark.

In the NC scheme, the real subprocesses are all the $jj \to \ell\nu\gamma j$ processes, where j stands for any parton. The POWHEG BOX separates automatically all singular regions of the real subprocesses. The regions characterized by a collinear parton j have an associated underlying Born with an $\ell\nu\gamma$ final state, while those characterized by a collinear photon have an underlying Born with an $\ell\nu j$ final state.

In the computation of the $\bar{B}$ function for the $q\bar{q}' \to \ell\nu\gamma$ subprocess, we include the strong soft-virtual corrections (the V term), the collinear remnants and the real contribution corresponding to a coloured parton becoming collinear in the $jj \to \ell\nu\gamma j$ real process. In the case of the $jj \to \ell\nu j$ underlying Born, the V term and the collinear remnants term, corresponding to electromagnetic corrections are set to zero. The real contribution, corresponding to the collinear photon region of the $jj \to \ell\nu\gamma j$ real process (also corresponding to an electromagnetic correction) is instead included.[9] In a variant of the C scheme that will be described later, all strong corrections to the $jj \to \ell\nu j$ underlying Born kinematics are also included.

As already recalled, in POWHEG the hardest radiation is generated through the modified Sudakov form factor, by evaluating the emission probability for all the allowed IR singular regions. In typical applications, this amounts to considering radiation from each coloured leg. The POWHEG BOX can be optionally instructed to also consider the singular regions arising from electromagnetic radiation, and in the case at hand we turn on this option. Thus IR singularities can originate from QCD radiation from partons, as well as from QED radiation off quarks and final-state leptons. This situation is somehow similar to what happens in the combined treatment of QCD and EW corrections to a given hadroproduction process, like e.g. the single W/Z production processes addressed in refs. [67, 68]. However, here the situation is much more complex because of the presence of two inequivalent underlying Born structures that refer to two different physical processes. If the singular region shows up in correspondence with a QCD radiation process, it will be driven by gluon bremsstrahlung or $g \to q\bar{q}$ collinear splitting in $W\gamma$ production, whose underlying Born structure is the direct photon contribution. On the other hand, when the IR singular configuration comes from an enhanced photon emission off partons/leptons, it will be originated by QED emission starting from an underlying Wj Born structure.

---

[9]The POWHEG BOX includes it automatically. However, excluding them (from the $\bar{B}$ function) completely would not spoil the accuracy of our calculation, since other corrections of the same order (i.e. the V term) are not included.

In POWHEG, the underlying Born kinematics and flavour is generated first with a probability proportional to the $\bar{B}$ function. Depending upon this choice, a coloured parton radiation or a photon radiation is generated at the subsequent stage. More precisely, our NC scheme is codified in the following POWHEG formula:

$$
\begin{aligned}
d\sigma = \sum_{f_b} \bar{B}_{W\gamma}^{f_b}(\mathbf{\Phi}_{\mathrm{B}})\, d\mathbf{\Phi}_{\mathrm{B}} &\left\{ \Delta^{f_b}(\mathbf{\Phi}_{\mathrm{B}}, p_{\mathrm{T}}^{\min}) \right. \\
&\left. + \sum_{\alpha_{\mathrm{r}} \in \{\alpha_{\mathrm{r}} | f_b\}} \frac{\left[d\Phi_{\mathrm{rad}}\, \theta\left(k_{\mathrm{T}} - p_{\mathrm{T}}^{\min}\right) \Delta^{f_b}(\mathbf{\Phi}_{\mathrm{B}}, k_{\mathrm{T}})\, R_{W\gamma;j}(\mathbf{\Phi}_{n+1}) \right]_{\alpha_{\mathrm{r}}}^{\bar{\mathbf{\Phi}}_n^{\alpha_{\mathrm{r}}} = \mathbf{\Phi}_{\mathrm{B}}}}{B_{W\gamma}^{f_b}(\mathbf{\Phi}_{\mathrm{B}})} \right\} \\
+ \sum_{f_b} {B'}_{Wj}^{f_b}(\mathbf{\Phi}_{\mathrm{B}})\, d\mathbf{\Phi}_{\mathrm{B}} &\left\{ \Delta^{f_b}(\mathbf{\Phi}_{\mathrm{B}}, p_{\mathrm{T}}^{\min}) \right. \\
&\left. + \sum_{\alpha_{\mathrm{r}} \in \{\alpha_{\mathrm{r}} | f_b\}} \frac{\left[d\Phi_{\mathrm{rad}}\, \theta\left(k_{\mathrm{T}} - p_{\mathrm{T}}^{\min}\right) \Delta^{f_b}(\mathbf{\Phi}_{\mathrm{B}}, k_{\mathrm{T}})\, R_{Wj;\gamma}(\mathbf{\Phi}_{n+1}) \right]_{\alpha_{\mathrm{r}}}^{\bar{\mathbf{\Phi}}_n^{\alpha_{\mathrm{r}}} = \mathbf{\Phi}_{\mathrm{B}}}}{B_{Wj}^{f_b}(\mathbf{\Phi}_{\mathrm{B}})} \right\} , \quad (2.6)
\end{aligned}
$$

where we use the notation $R_{W\gamma;j}^{\alpha_{\mathrm{r}}}/R_{Wj;\gamma}^{\alpha_{\mathrm{r}}}$ to denote the contributions to $R_{W\gamma j}$ that are singular only when a parton/photon is collinear. Thus, the first two lines of eq. (2.6) are associated to the direct photon contribution (i.e. to the $W\gamma$ underlying Born) and the last two lines refer to radiative photon contribution (with the Wj underlying Born). Note that the $R_{W\gamma;j}$ term has only one singular region, corresponding to a radiated parton collinear to the beam axis, while the $R_{Wj;\gamma}$ has two singular regions, one corresponding to a radiated photon collinear to the beam axis, and the other corresponding to a photon collinear to the lepton.

In the $\bar{B}_{W\gamma}^{f_b}$ term the NLO QCD corrections to the inclusive cross section of the direct photon production process are included, while ${B'}_{Wj}^{f_b}$ has a formal structure similar to eq. (2.4) but with the (QED-like) finite part $V(\mathbf{\Phi}_{\mathrm{B}})$ (and collinear remnants) set to zero. For the remaning QED terms we employ the ingredients already available in the POWHEG BOX for the treatment of the EW corrections to single vector boson production [67, 68]. Therefore, we do not take into account the full NLO EW corrections to the Wj process. These corrections are of α_{em} relative order, and are therefore subleading. In all cases, they are certainly much smaller than the strong corrections to the Wj process.

2.3.3 Implementation of the NC scheme

The NC realization thus proceeds according to the following algorithm automated in the POWHEG BOX:

1. generate an underlying Born kinematics according to the probability distribution

$$
\mathrm{d}\Phi_{\mathrm{B}} \bar{B}_{\mathrm{tot}} = \mathrm{d}\Phi_{\mathrm{B}} \left(\bar{B}_{W\gamma}^{f_b} + {B'}_{Wj}^{f_b} \right) , \tag{2.7}
$$

then select a direct photon production or a radiative photon contribution with probability proportional to $\bar{B}_{W\gamma}^{f_b}(\Phi_B)$ and $B'^{f_b}_{Wj}(\Phi_B)$;

2. once one of the two underlying Born process has been selected, generate the hardest radiation using the corresponding Sudakov form factor. Observe that in case of the $W\gamma$ underlying Born the Sudakov form factor refers to QCD emission (i.e. to the $R_{W\gamma;j}$ emission), while for the Wj underlying Born it refers to QED emission (i.e. to the $R_{Wj;\gamma}$ emission);

3. in case of events from $\bar{B}_{W\gamma}^{f_b}$, proceed as in the default `POWHEG` method: the variable `SCALUP` is set to the transverse momentum of the radiated parton, or to $p_T^{\min}$ if no radiation occurs, and the event is passed to the shower generator;

4. in case of events from $B'^{f_b}_{Wj}$, set `SCALUP` to the transverse momentum of the parton in the underlying Born process, and pass the event to the shower (notice that the default `POWHEG` behaviour would instead set `SCALUP` to the transverse momentum of the photon).

In the NC procedure, a photon is always generated at the `POWHEG` level. It is thus not necessary to turn on QED radiation in the Shower generator. If QED radiation is turned on in the Shower, care must be taken to veto QED radiation harder than `SCALUP`, as detailed in the following.

It is useful to see how the full phase space for photon radiation is generated, without overcounting with this procedure:

- in case of events from a $\bar{B}_{W\gamma}^{f_b}$ underlying Born, we generate events where *the photon is harder than any other parton* (i.e. jet) in the event. By hardness we mean here the p_T relative to all other particles that could have emitted the photon or parton, including the incoming ones. One further parton, softer than the photon, is (generally) generated by `POWHEG`. The value of `SCALUP` is set to the transverse momentum of this radiation, and the shower generates radiation softer than `SCALUP`;

- in case of events from $B'^{f_b}_{Wj}$, an event is generated first with the *the photon softer than at least one emitted parton*. Since `SCALUP` is set in this case to the transverse momentum of the parton in the underlying Born kinematics, and the photon is softer than this parton, the shower may still generate parton that are harder than the photon, but softer than the initial, underlying Born parton.

Notice that if we had followed the standard `POWHEG` procedure for setting `SCALUP`, we would have ended up with events where the photon is the second hardest parton with a probability that is not suppressed by α_{em}. In fact, the underlying Born cross section for the Wj process does not carry a QED coupling, and the Sudakov mechanism for photon emission guarantees that one photon is always emitted (or at least it would do so if the IR cutoff for photon emission was set to zero), and no parton harder than the photon could be produced. This is clearly unphysical. If we suppress parton radiation, a corresponding

Sudakov form factor should also be present, and we don't have it in this case. This is why we must allow harder parton radiation, by a different setting of the `SCALUP` value.

As mentioned earlier, the NC approach to the NLOPS simulation of the $W\gamma$ process closely resembles the `POWHEG`-like method developed in ref. [39] for the diphoton production process. That work is carried out in the framework of `Herwig++` [69], and truncated shower are provided there to cope more accurately with the shower matching needed in the case of angular ordered parton showers. Also in ref. [39], events with one less photon and an extra parton (i.e. the $j\gamma$ Born subprocess for the $\gamma\gamma$ final state) are allowed to shower from the initial scale, using truncated showers, vetoing QED radiation harder than the generated photon, but imposing no veto on the QCD radiation. Our NC approach is thus equivalent, since truncated showers are not needed in the p_T ordered showers generators `PYTHIA` v.6 and v.8 [70, 71] that we are using.

2.3.4 Implementation of the C scheme

In the NC scheme, in the generation of Wj events, while the QED radiation is emitted using exact tree level matrix elements, QCD radiation harder than the photon is emitted by the shower in the collinear approximation. This is bound to spoil the accuracy of the QED emission matrix element, since harder QCD radiation may throw off shell the propagator of the photon-emitting parton by a larger amount than the corresponding QED radiation. We thus consider a more accurate description, corresponding to our C scheme, codified by the following formula

$$
\begin{aligned}
d\sigma = \sum_{f_b} \bar{B}_{W\gamma}^{f_b}(\mathbf{\Phi}_B)\, d\mathbf{\Phi}_B \Bigg\{ &\Delta^{f_b}\big(\mathbf{\Phi}_B, p_T^{\min}\big) \\
&+ \sum_{\alpha_r \in \{\alpha_r | f_b\}} \frac{\left[d\Phi_{\rm rad}\, \theta\left(k_T - p_T^{\min}\right) \Delta^{f_b}(\mathbf{\Phi}_B, k_T)\, R_{W\gamma;j}\left(\mathbf{\Phi}_{n+1}\right)\right]_{\alpha_r}^{\bar{\mathbf{\Phi}}_n^{\alpha_r}=\mathbf{\Phi}_B}}{B_{W\gamma}^{f_b}(\mathbf{\Phi}_B)} \Bigg\} \\
+ \sum_{f_b} B'^{f_b}_{Wj}(\mathbf{\Phi}_B)\, d\mathbf{\Phi}_B \Bigg\{ &\Delta^{f_b}\big(\mathbf{\Phi}_B, p_T^{\min}\big) \\
&+ \sum_{\alpha_r \in \{\alpha_r | f_b\}} \frac{\left[d\Phi_{\rm rad}\, \theta\left(k_T - p_T^{\min}\right) \Delta^{f_b}(\mathbf{\Phi}_B, k_T)\, R_{Wj;\gamma}\left(\mathbf{\Phi}_{n+1}\right)\right]_{\alpha_r}^{\bar{\mathbf{\Phi}}_n^{\alpha_r}=\mathbf{\Phi}_B}}{B_{Wj}^{f_b}(\mathbf{\Phi}_B)} \\
&+ \sum_{\alpha_r \in \{\alpha_r | f_b\}} \frac{\left[d\Phi_{\rm rad}\, \theta\left(k_T - p_T^{\min}\right) \Delta^{f_b}(\mathbf{\Phi}_B, k_T)\, R_{Wj;j}\left(\mathbf{\Phi}_{n+1}\right)\right]_{\alpha_r}^{\bar{\bar{\mathbf{\Phi}}}_n^{\alpha_r}=\mathbf{\Phi}_B}}{B_{Wj}^{f_b}(\mathbf{\Phi}_B)} \Bigg\} .
\end{aligned} \tag{2.8}
$$

In the second term of eq. (2.8) the Sudakov form factor has now the form

$$
\Delta^{f_b}(\mathbf{\Phi}_{\mathrm{B}}, p_{\mathrm{T}}) = \exp \left\{ - \sum_{\alpha_{\mathrm{r}} \in \{\alpha_{\mathrm{r}} | f_b\}} \int \frac{\left[d\Phi_{\mathrm{rad}}\, R_{Wj;\gamma}\left(\mathbf{\Phi}_{n+1}\right) \theta\left(k_{\mathrm{T}}(\mathbf{\Phi}_{n+1}) - p_{\mathrm{T}}\right) \right]_{\alpha_{\mathrm{r}}}^{\bar{\mathbf{\Phi}}_n^{\alpha_{\mathrm{r}}} = \mathbf{\Phi}_{\mathrm{B}}}}{B^{f_b}\left(\mathbf{\Phi}_{\mathrm{B}}\right)} \right\}
$$

$$
\times \exp \left\{ - \sum_{\alpha_{\mathrm{r}} \in \{\alpha_{\mathrm{r}} | f_b\}} \int \frac{\left[d\Phi_{\mathrm{rad}}\, R_{Wj;j}\left(\mathbf{\Phi}_{n+1}\right) \theta\left(k_{\mathrm{T}}(\mathbf{\Phi}_{n+1}) - p_{\mathrm{T}}\right) \right]_{\alpha_{\mathrm{r}}}^{\bar{\mathbf{\Phi}}_n^{\alpha_{\mathrm{r}}} = \mathbf{\Phi}_{\mathrm{B}}}}{B^{f_b}\left(\mathbf{\Phi}_{\mathrm{B}}\right)} \right\} .
$$

$$(2.9)$$

Thus, in case of the Wj underlying Born, QCD radiation competes with QED radiation. Because of the larger value of the QCD coupling constant QCD radiation will be more frequent. In case of QCD emission from Wj dynamics, the photon may only emerge from the subsequent PS, where interleaved QED evolution must be turned on. The recipe for the C scheme is thus as follows:

1. generate an underlying Born kinematics according to the probability distribution

$$
\mathrm{d}\Phi_{\mathrm{B}} \bar{B}_{\mathrm{tot}} = \mathrm{d}\Phi_{\mathrm{B}} \left(\bar{B}_{W\gamma}^{f_b} + B'^{f_b}_{Wj} \right) ,
$$

$$(2.10)$$

   then select a direct photon production or a radiative photon contribution with probability proportional to $\bar{B}_{W\gamma}^{f_b}(\Phi_{\mathrm{B}})$ and $B'^{f_b}_{Wj}(\Phi_{\mathrm{B}})$;

2. if the $W\gamma$ case is selected, radiation is performed (as in the NC scheme) according to the QCD Sudakov form factor for the emission of an additional parton. The subsequent PS is vetoed according to the standard `POWHEG SCALUP` value, set to the p_{T} of the emitted parton. Since in this case the PS must be used with interleaved QED evolution turned on, care must be taken to veto photon radiation with transverse momenta above `SCALUP`;

3. if the Wj case is selected, both QED or QCD radiation can be generated. In this way, photon emission off partons turns out to be inhibited by the competing QCD radiation. In case of QCD emission the photon can only arise from the subsequent PS evolution, that must be fully turned on, with electromagnetic radiation that can arise from the final state lepton and from the incoming and outgoing quarks. Also in this case `SCALUP` is set according to the standard `POWHEG` prescription both for photon and parton radiation, and care must be taken to veto photon emission (generated by the PS) harder than `SCALUP`;

4. concerning the accuracy of the Wj contribution, we adopt in our formulation two possible options: *i)* a LO accuracy of the W plus one jet process; *ii)* a NLO accuracy, obtained by the inclusion of the full, NLO accurate $\bar{B}_{Wj}^{f_b}$ instead of $B'^{f_b}_{Wj}$. The difference between the results of these two variants will be shown and discussed in section 3. We will label the two variants as C-LO and C-NLO. All the above improvements were easily implemented using the routines already available in the `POWHEG BOX` for the simulation of the vector boson plus one jet production process [72].

A clear representation of the role of the various contributions adopted in our C scheme is given below:

- Contributions with gluon radiation from a $W\gamma$ underlying Born configuration: these correspond to the case when *the hardest particle among all final state partons and photons is a photon.*

- Contributions with a photon radiated from a Wj underlying Born configuration: these correspond to the case when *the hardest particle among all final state partons and photons is a coloured parton; the second hardest one is a photon.*

- Contributions with a parton radiated from a Wj underlying Born configuration: these correspond to the case when *the first two hardest particles among all final state partons and photons are coloured partons.* In this sample, the shower has to generate correctly the cases when the photon is the third, fourth, and so on, hardest particle, up to the case when no photon is emitted at all.

It is clear now that in order to correctly describe all the classes of events corresponding to the third item above, the usage of an interleaved QCD+QED PS is mandatory.

We remark that the C scheme differs from the NC scheme (and thus also from the approach of D'Errico and Richardson [39]) by the treatment of the second parton radiation. In the C scheme, when the second parton radiation is harder than the photon radiation, the photon is generated by the PS (in the collinear approximation) while the parton is generated with matrix element accuracy. Conversely, in the NC scheme it can happen that a second parton harder than the photon is emitted by the PS in the collinear approximation, while the photon was accurate at the matrix element level. This is clearly incorrect, since in this case the momentum of the radiated second parton would heavily affect the matrix element for photon radiation.

The C scheme is our novel proposal for the treatment of a prompt-photon process. This scheme guarantees that photon emission is treated consistently even if the photon is softer than a certain number of QCD partons. We will see in the following that the emission of a photon softer than other QCD partons in the event can give sizeable contributions to realistic observables, and thus a consistent treatment of these events leads to an improved description of the process.

Our C-NLO scheme, based upon the usage of the Wjj matrix elements and NLO accuracy of the Wj process interfaced to a QCD+QED interleaved shower, goes beyond the required accuracy of our generator, and goes in fact in the direction of a calculation of the $W\gamma$ process at NNLO accuracy. Nevertheless, in view of the large NLO corrections to the Wj process, and in view of the fact that this subprocess contributes to a precise slice of phase space of the whole process (i.e. no other subprocess can accidentally cancel its contribution), we believe that the inclusion of its NLO corrections is justified. We also notice that, formally, when computing NLO corrections to prompt photon production processes at fixed order using the fragmentation function formalism, the fragmentation component should also be evaluated at the NLO level. In fact, the fragmentation function

is of order $\alpha_{\rm em}/\alpha_{\rm S}$, so that at the Born level the direct and fragmentation components are formally of the same accuracy.

2.4 The MiNLO procedure

As described in the previous sections, the simulation of the $W\gamma$ signature rests on the calculation of LO and NLO matrix elements describing W production in association with real photon and jet radiation. These radiation processes contain singularities associated with the emission of soft and collinear partons or photons which, in the absence of the virtual counterpart, prevent an integration of the related matrix elements over the full phase space.

The LO $W\gamma$ matrix element is characterized by the presence of singularities associated with the emission of soft and collinear photons off the partons and off the final state lepton from W decay. This requires the introduction of generation cuts that prevent the singular regions from being probed, that must be chosen much smaller than the cuts applied at the analysis level. In analogy to the POWHEG treatment of the Vj process [72], we require in the simulation of the $W\gamma$ contribution the presence of a generation cut of order $p_{\rm T}^{\gamma,\rm min} = 1\,{\rm GeV}$ and $\Delta R_{\ell\gamma}^{\rm min} = 0.1$, that are definitely smaller than the typical cuts imposed on the isolated photon, generally required to be sufficiently hard (with $p_{\rm T}^{\gamma} \geq 10\,{\rm GeV}$), and well separated from the lepton. This simple procedure guarantees that the results of the calculation are stable against variations of the applied experimental cuts in the case of realistic event selections. Of course, this treatment of the phase space turns out to be effective and does not introduce any bias in the theoretical predictions since the generation cuts are imposed in a sufficiently loose way on the same particle (the photon) which is at the end more strongly constrained at the analysis level.

In our approach to $W\gamma$ production, however, a problem arises due to the partitioning of the final state phase space that we adopt. Let us consider photons arising from W decays. They will mostly have a small relative $p_{\rm T}$ of the photon-lepton system. Events of this kind arising from the $W\gamma$ underlying Born will be treated by POWHEG as small $p_{\rm T}$ events, and will thus have a small SCALUP value, such that not much further radiation will be allowed in the shower. On the other hand, events of the same kind may also arise with Wj as underlying Born. In the limit of small transverse momentum of the emitted jet, the divergent underlying Born will end up giving a sizeable contribution to this kind of events. In fact, as the transverse momentum of the underlying Born jet is reduced, the suppression of photon radiation (due to the reduction of the region where the photon-lepton $p_{\rm T}$ is smaller than the jet $p_{\rm T}$) will compensate the enhancement of the underlying Born, leaving a significant contribution. Notice that photon radiation off quarks will be irrelevant in this case, since it will not pass the requirement of a hard photon. On the other hand, radiation from the lepton may still be capable to yield photons with a hard $p_{\rm T}$ with respect to the beam axis. If we require a minimum ΔR separation between the photon and the lepton, a small relative transverse $p_{\rm T}$ of the lepton-photon system will only be possible if the lepton is soft (we don't consider a soft γ, since that will not pass our cuts). We find that, even in this case, the phase space suppression of this region is not sufficient to fully compensate the diverging underlying Born cross section, leaving a finite contribution characterized by

a hard photon and a soft lepton, that strongly depends upon the generation cut for the Wj kinematics.

In order to tackle this problem, and to provide a generator able to give predictions under general event selection conditions, we resort to the MiNLO procedure [35, 36]. MiNLO can be seen as an NLO extension of the matrix element reweigthing method used in tree-level matrix element-PS merging algorithms [73–76]. It has been already applied to the simulation of Higgs and vector boson production in association with up to two jets [36, 77] and to $HW/HZ+1$ jet [78]. In the MiNLO method, the calculation of an inclusive cross section is modified by the inclusion of Sudakov form factors and by making appropriate choices for the scales of the the strong coupling constants associated with each emission vertex.

In our case, we apply the MiNLO procedure in analogy to the case of the Vj generator [36]. However, we need to specify a slightly different procedure for the treatment of the $W\gamma$ contribution.

For Wj production at NLO (as in our C-NLO scheme) the application of the MiNLO procedure is exactly the same as in [36]. For Wj at LO, B'_{Wj} is modified according to the following formula

$$
\begin{aligned}
B'_{Wj} &= B_{Wj} + \int d\Phi_{\text{rad}} R_{Wj;\gamma} \\
&\to B_{Wj} \times \frac{\alpha_{\text{S}}(p_{\text{T}})}{\alpha_{\text{S}}} \Delta^2(M_{W^*}, p_{\text{T}}) + \int d\Phi_{\text{rad}} \frac{\alpha_{\text{S}}(p_{\text{T}})}{\alpha_{\text{S}}} \Delta^2(M_{W^*}, p_{\text{T}}) R_{Wj;\gamma}, \quad (2.11)
\end{aligned}
$$

where M_{W^*} is the virtuality of the W boson, i.e. $M_{W^*}^2 = (p_\ell + p_\nu)^2$, and $p_{\text{T}} = (p_\ell + p_\nu)_{\text{T}}$, and α_{S} in the denominator is evaluated at the same scale as in the B_{Wj} term (in other words, the α_{S} coupling in B_{Wj} is replaced by $\alpha_{\text{S}}(p_{\text{T}})$). A modification with the same formal structure as in eq. (2.11) is applied in the calculation of the real radiation matrix element of the $Wj\gamma$ production process, where p_{T} is the transverse component of $(p_\ell + p_\nu)$ computed according to the real radiation kinematics. In eq. (2.11) the Sudakov form factor Δ is given by

$$
\Delta(Q, p_{\text{T}}) = \exp\left\{ -\int_{p_{\text{T}}^2}^{Q^2} \frac{dq^2}{q^2} \left[A\left(\alpha_{\text{S}}(q^2)\right) \log \frac{Q^2}{q^2} + B\left(\alpha_{\text{S}}(q^2)\right) \right] \right\}, \quad (2.12)
$$

where the functions A and B have a perturbative expansion in terms of constant coefficients

$$
A(\alpha_{\text{S}}) = \sum_{i=1}^{\infty} A_i \, \alpha_{\text{S}}^i, \qquad B(\alpha_{\text{S}}) = \sum_{i=1}^{\infty} B_i \, \alpha_{\text{S}}^i. \quad (2.13)
$$

In MiNLO only the coefficients A_1, A_2, B_1 and B_2 are needed and their expression can be found in ref. [36]. At the NLO accuracy, the Wj inclusive cross section is treated according to the formula

$$
\begin{aligned}
\bar{B}_{Wj} \longrightarrow &\frac{\alpha_{\text{S}}(p_{\text{T}})}{\alpha_{\text{S}}} \Delta^2(M_{W^*}, p_{\text{T}}) \left[B_{Wj}\left(1 - 2\Delta^{(1)}\right) + \frac{\alpha_{\text{S}}(p_{\text{T}})}{\alpha_{\text{S}}} \left(V + \int \frac{dz}{z} G\right) \right] \\
&+ \int d\Phi_{\text{rad}} \frac{\alpha_{\text{S}}(p_{\text{T}})}{\alpha_{\text{S}}} \Delta^2(M_{W^*}, p_{\text{T}}) \left[\frac{\alpha_{\text{S}}(p_{\text{T}})}{\alpha_{\text{S}}} R_{Wjj} + R_{Wj;\gamma} \right], \quad (2.14)
\end{aligned}
$$

where M_{W^*} and p_T have the same meaning as in eq. (2.11), again with the only difference that for the real radiation matrix element $R \equiv |M_{Wjj}|^2$ the variable p_T is derived according to the real radiation kinematics. In eq. (2.14) $\Delta^{(1)}$ is the $\mathcal{O}(\alpha_S)$ expansion of the Sudakov form factor

$$\Delta^{(1)}(Q, p_T) = \alpha_S(p_T) \left[-\frac{1}{2} A_1 \log^2 \frac{p_T^2}{Q^2} + B_1 \log \frac{p_T^2}{Q^2} \right], \tag{2.15}$$

which is subtracted in order to maintain NLO accuracy.

Concerning the $W\gamma$ direct photon contribution, we proceed as follows. Since the $W\gamma$ contribution can be regarded as a configuration where no parton is emitted with transverse momentum larger than that of the photon, the photon p_T provides an upper limit for the partonic emission, and the proper reweighting for the LO inclusive cross $B_{W\gamma}$ is

$$B_{W\gamma} \longrightarrow B_{W\gamma} \times \Delta^2(M_{W^*}, p_T), \tag{2.16}$$

where we choose the scales p_T and M_{W^*} taking care of the distinction between initial-state (ISR) and final-state photon radiation (FSR). For ISR, M_{W^*} will be closer to the lepton-neutrino invariant mass and therefore $M_{W^*}^2 = (p_\ell + p_\nu)^2$ and $p_T = (p_\ell + p_\nu)_T$. For FSR, M_{W^*} will be closer to the invariant mass of the lepton-neutrino-gamma system: therefore, we choose $M_{W^*}^2$ as $(p_\ell + p_\nu + p_\gamma)^2$ and the correct upper limit for partonic emission is here represented by the relative lepton-photon transverse momentum, for which we use the expression

$$p_\gamma \cdot p_\ell \frac{E_\gamma E_\ell}{(E_\gamma + E_\ell)^2} \tag{2.17}$$

computed in the partonic CM system, for reasons that will be soon clarified. At the NLO accuracy, the $W\gamma$ inclusive cross section is treated according to the following formula [35, 36]

$$\bar{B}_{W\gamma} \longrightarrow \Delta^2(M_{W^*}, p_T) \left[B_{W\gamma} \left(1 - 2\Delta^{(1)} \right) + \frac{\alpha_S(p_T)}{\alpha_S} \left(V + \int \frac{dz}{z} G \right) \right]$$
$$+ \int d\Phi_{rad} \frac{\alpha_S(p_T)}{\alpha_S} \Delta^2(M_{W^*}, p_T) R_{W\gamma;j}, \tag{2.18}$$

where the meaning of M_{W^*} and p_T is the same as in eq. (2.16), with the only difference that for the real radiation matrix element $R \equiv |M_{W\gamma j}|^2$ p_T is calculated according to real radiation kinematics.

Notice that the $\Delta^{(1)}$ term in eq. (2.18) contains Sudakov logarithms that should cancel against similar logarithms arising in the last term of the equation from the $\int d\Phi_{rad} R_{W\gamma;j}$ integral.[10] As far as FSR is concerned, in this integral the radiation phase space is restricted by the fact that $R_{W\gamma;j}$ is suppressed when the radiation transverse momentum is larger than the relative lepton-photon transverse momentum, defined according to the default POWHEG BOX internal mechanism for the separation of singular regions [34], and corresponding precisely to the definition in eq. (2.17), that thus ensures that these large logarithms are fully cancelled, and correctly exponentiated.

---

[10]We remind the reader that $R_{W\gamma;j}$ is singular, and that the singularities are regulated by "+" distributions, so that by integrating it Sudakov logarithms can arise as usual from phase space restrictions.

Thanks to the MiNLO procedure, we are thus able to provide a generator that covers all the transverse momentum regions. We stress that, because of the non perturbative behaviour of the strong coupling constant in the low energy regime, a minimum cut on the parton or W transverse momentum, say $p_{\mathrm{T}}^{j,\mathrm{min}} = 1\,\mathrm{GeV}$, must be necessarily introduced at the generation level. However, it does not play the rôle of a fictitious, unphysical cutoff as a consequence of the smooth and vanishing behaviour of the Sudakov form factor in the limit $p_{\mathrm{T}} \to 0$, which renders the predictions independent of the specific $p_{\mathrm{T}}^{j,\mathrm{min}}$ choice for sufficiently small $p_{\mathrm{T}}^{j,\mathrm{min}}$ values.

2.5 Interface to a shower generator

The interface to the shower generator requires different kinds of vetoes in the `POWHEG`-C and in the `POWHEG`-NC cases:

- `POWHEG`-C: in this case `SCALUP` is set to the hardest emission, whether it is a parton (arising from the $W\gamma$ or Wj underlying Born) or a photon (Wj underlying Born). The mixed QED+QCD shower must be turned on.

- `POWHEG`-NC: in this case, for events from the $W\gamma$ underlying Born, `SCALUP` is set to the hardest parton emission, as in the default `POWHEG` method. In the Wj underlying Born case, `SCALUP` should instead be set to the transverse momentum of the underlying Born parton. It is not strictly necessary to turn on a full QED+QCD shower in this case, since the hardest photon is already generated at the Les Houches event level. If the QED shower is active, we must require that no photons are generated harder then the Les Houches photon.

Shower MC generators do not in general enforce a veto on the transverse momentum of photons radiated by the leptons, irrespective of the value of `SCALUP`. In `PYTHIA` v.8, it is possible to set a flag such that `SCALUP` veto is imposed also in this case. In `PYTHIA` v.6 no such option exists. We thus implement the photon veto at the analysis level. We compute the relative transverse momentum of the lepton-photon system after shower in the laboratory frame, defined as

$$p_{\ell\gamma}^{\mathrm{rel}} = 2E_\gamma \sin\frac{\theta_{\ell\gamma}}{2}\,, \tag{2.19}$$

for the first final-state shower generated photon arising from the lepton. It is required that $p_{\ell\gamma}^{\mathrm{rel}}$ is smaller than `SCALUP`, and the showering stage is repeated keeping the same Les Houches event until this condition is satisfied.

3 Phenomenological results

In the present section, we show and discuss the numerical results obtained with the new tool. First, we show some comparisons with the NLO MC program `MCFM`, which is the reference code for $W\gamma$ production studies at the LHC. Then, we provide our phenomenological results for a number of differential cross sections of interest for physics studies at the Run II of the LHC, and discuss the results of the different `POWHEG`+MiNLO realizations

described in section 2.3.2 and section 2.4 in comparison to NLO calculations. Finally, we compare our predictions with the measured cross sections at the LHC at 7 TeV.

3.1 Comparisons to MCFM: integrated cross sections

We present a comparisons of our NLOPS generator and MCFM considering the following cases:

1. comparisons at pure NLO accuracy, using the smooth isolation approach as photon isolation procedure. This eliminates the fragmentation contribution and allows us to check our implementation of the NLO QCD corrections to direct photon production;

2. comparisons between the NLO predictions of MCFM and the full results of our simulations. In this comparisons we use a realistic photon isolation cut, and thus the MCFM result depends upon the photon fragmentation function. We provide our predictions in terms of the POWHEG-NC, POWHEG-C-LO and POWHEG-C-NLO realizations.

While in the first case we expect exact agreement, in the second case differences will show up necessarily because of the different content of our approach.

The results presented here are obtained using the latest version of the MCFM code, i.e. MCFM v6.8. We used the following set of EW input parameters

$$M_W = 80.385 \text{ GeV} \qquad M_Z = 91.1876 \text{ GeV} \qquad G_\mu = 1.1663787 \times 10^{-5} \text{ GeV}^{-2} \quad (3.1)$$
$$\Gamma_W = 2.085 \text{ GeV} \qquad \alpha_{\text{em}}(0) = 1/137.035999074 \,. \tag{3.2}$$

We compute the $O(\alpha_{\text{em}}^3)$ LO cross section using for the electromagnetic coupling constant the expression

$$\alpha_{G_\mu} = \frac{\sqrt{2}\, G_\mu\, M_W^2 \sin^2 \theta_W}{\pi} \,, \tag{3.3}$$

with $\sin^2 \theta_W = 1 - M_W^2/M_Z^2$, and we rescale the results by the factor $\alpha_{\text{em}}(0)/\alpha_{G_\mu}$ to account for the correct coupling to the on-shell photon. For definiteness, we use the NLO PDF set CTEQ10 [79] (any other modern set can equivalently be used [80, 81]). For the fragmentation of partons into photons, needed by the MCFM code, the parameterization "Set II" of ref. [61] was used.

Similarly to the analysis performed in ref. [19], as well as to cover the main event selection conditions of interest at the LHC, we consider both in comparison 1 and 2 the following three sets of cuts

$$\text{Basic Photon} - p_{\text{T}}^\gamma > 15 \text{ GeV}, \quad |\eta_\gamma| < 2.37, \quad \Delta R_{\ell\gamma} > 0.7, \quad R_0 = 0.4, \quad \epsilon_h = 0.5 \quad (3.4\text{a})$$
$$M_T \text{ cut} - \text{Basic Photon} + M_T > 90 \text{ GeV} \tag{3.4b}$$
$$\text{Lepton cuts} - \text{Basic Photon} + p_{\text{T}}^\ell > 25 \text{ GeV}, \quad |\eta_\ell| < 2.47, \quad p_{\text{T}}^\nu > 35 \text{ GeV} \,, \tag{3.4c}$$

where R_0 and ϵ_h are the parameters defining the isolation criterion, as defined further on. They give rise to quite different K-factors [19] and therefore allow us to perform a

non-trivial test of our calculation. In eq. (3.4b), M_T is the transverse mass of the photon-lepton-missing transverse energy system, defined as

$$M_{T,\ell\nu\gamma}^2 = \left(\sqrt{m_{\ell\gamma}^2 + |\mathbf{p}_T^\gamma + \mathbf{p}_T^\ell|^2} + E_T^\nu\right)^2 - |\mathbf{p}_T^\gamma + \mathbf{p}_T^\ell + \mathbf{E}_T^\nu|^2 , \qquad (3.5)$$

where $m_{\ell\gamma}$ is the invariant mass of the photon-lepton system. A M_T cut is particularly useful since it suppresses the contribution of photons radiated by the lepton in the W decay, which is of no interest for the studies of ATGCs and for the observation of radiation zeros. The basic photon cuts defined in eq. (3.4a) mimic the criteria adopted by the CMS collaboration in the comparison of MCFM to the data at $\sqrt{s} = 7\,\text{TeV}$,[11] while the lepton in eq. (3.4c) resemble the experimental configuration used by ATLAS in the comparison between data and theoretical predictions at $\sqrt{s} = 7\,\text{TeV}$. Moreover, the conditions in eq. (3.4c), including an additional cut on the transverse mass of the $\ell\nu\gamma$ or $\ell\nu$ system, are similar to the selection criteria applied by ATLAS and CMS, respectively, to define the $W\gamma$ sample.

3.1.1 NLO comparison

We present results for the final state $e^+\nu\gamma$, using a central scale choice of $\mu_R = \mu_F = M_W$. The fragmentation scale is kept equal to M_W. We apply the following isolation prescription to the photon [65]

$$\forall_{R<R_0} \sum_{R_{j,\gamma}<R} E_{T,j} < \epsilon_h\, p_T^\gamma \left(\frac{1 - \cos R}{1 - \cos R_0}\right) , \qquad (3.6)$$

where $E_{T,j}$ is the transverse energy of the final state parton j, and $R_{j\gamma} = \sqrt{\Delta\eta_{j\gamma}^2 + \Delta\phi_{j\gamma}^2}$ is the "separation" between the photon and a parton j. In case of the NLO calculation, only one parton is present in the final state, and the isolation condition can be simply stated as

$$\theta(R_0 - R_{j,\gamma})\, E_{T,j} < \epsilon_h\, p_T^\gamma \left(\frac{1 - \cos R_{j,\gamma}}{1 - \cos R_0}\right) , \qquad (3.7)$$

where j here stands for the single final state parton. We used the values $\epsilon_h = 0.5$ and $R_0 = 0.4$ for the isolation parameters.

The results of the comparisons are shown in table 1 and 2 for $\sqrt{s} = 7\,\text{TeV}$ and $\sqrt{s} = 14\,\text{TeV}$, respectively. As can be seen, the predictions of MCFM and POWHEG agree within the statistical uncertainty of the respective MC errors, given by the numbers in parenthesis. For completeness, we also checked that the distributions obtained with the two calculations are in good agreement. Thus, in the absence of the fragmentation contribution, the two calculations of the NLO QCD corrections to $W\gamma$ production nicely agree.

3.1.2 Full comparison

In our full comparison between our NLOPS simulations and the MCFM results, photon isolation is implemented by requiring that the transverse hadronic energy inside R_0 is

---

[11]Strictly speaking, in the criteria adopted by CMS no acceptance cuts on the lepton are applied and the photon isolation requirements are more complex than those as in eq. (3.4a).

Cuts	MCFM	POWHEG NLO
Basic Photon	13.12(4)	13.15(1)
M_T cut	2.770(1)	2.774(3)
Lepton cuts	1.126(1)	1.123(4)

Table 1. Comparison between MCFM and POWHEG NLO cross sections (in pb) of the $pp \to e^+ \nu \gamma$ process at $\sqrt{s} = 7 \, \mathrm{TeV}$, using the smooth isolation procedure, parameters and cuts described in the text. The numbers in parenthesis are the 1σ MC errors on the last digit. The results are the central value predictions for $\mu_R = \mu_F = M_W$.

Cuts	MCFM	POWHEG NLO
Basic Photon	23.90(8)	24.04(3)
M_T cut	6.230(2)	6.250(9)
Lepton cuts	2.342(2)	2.340(6)

Table 2. The same as table 1 at $\sqrt{s} = 14 \, \mathrm{TeV}$.

limited by the following condition

$$\sum_{R_{j,\gamma} < R_0} E_{T,j} < \epsilon_h \, p_\mathrm{T}^\gamma \,, \tag{3.8}$$

where j runs over all the final state particles except the photon and the electron, with $R_0 = 0.4$ and $\epsilon_h = 0.5$, as before. The shower program ensures that no QCD radiation will be generated harder than the SCALUP value. We enforce an analogous limitation on the radiation of photons: for a given Les Houches event, we repeat the shower stage if a photon harder then SCALUP is generated. We do not take into account in our simulations the contribution of secondary photons from the main radiative decays of hadrons, because they are normally treated as background.

In order to make contact with the MCFM formulation, we switch off in the shower generator the contribution of the underlying event, thus including only the shower and hadronization stages. In order to further minimize the possible sources of discrepancies, we require in our simulations that the charged lepton defining the signature is identified as the hardest lepton in the event sample and assume that the isolated photon coincides with the hardest photon among all the isolated ones.[12] Moreover, we require a calorimetric-like definition for the final state lepton, i.e. a lepton+photon recombination requirement for the photons generated by the QED PS, consistently with the dressed lepton definition inherent in MCFM. The latter requirement is imposed by setting the parameter PTminChgL $= 1 \, \mathrm{GeV}$ in PYTHIA v.8. Our results are obtained with PYTHIA v.8 as PS generator but we checked that no substantial differences (at $\sim 1\%$ level) are introduced when using PYTHIA v.6.

The comparisons between our full predictions and those of MCFM are given in table 3 and table 4 for $\sqrt{s} = 7 \, \mathrm{TeV}$ and $\sqrt{s} = 14 \, \mathrm{TeV}$, respectively. We include the MCFM theoretical

---

[12]We checked in our simulations that no appreciable differences are present if the lepton, as well as the isolated photon (whenever possible), are identified according to the MC truth.

Cuts	MCFM	POWHEG-NC	POWHEG-C-LO	POWHEG-C-NLO
Basic Photon	$12.92(3)^{+4\%}_{-6\%}$	$12.40(3)^{+8\%}_{-10\%}$	$12.95(3)^{+8\%}_{-11\%}$	$15.08(7)^{+2\%}_{-9\%}$
M_T cut	$2.625(1)^{+6\%}_{-6\%}$	$3.09(2)^{+10\%}_{-11\%}$	$3.20(2)^{+11\%}_{-11\%}$	$4.23(3)^{+10\%}_{-10\%}$
Lepton cuts	$1.077(1)^{+6\%}_{-6\%}$	$1.22(1)^{+8\%}_{-10\%}$	$1.31(1)^{+11\%}_{-11\%}$	$1.75(2)^{+7\%}_{-13\%}$

Table 3. Comparison between the NLO cross section predictions (in pb) of MCFM using photon fragmentation functions and the three different POWHEG+MiNLO implementations realized in this work, for the $pp \to e^+\nu\gamma$ process at $\sqrt{s} = 7$ TeV. Photon isolation conditions, parameters and cuts are specified in the text. The basic theoretical ingredients underlying the acronyms POWHEG-NC, POWHEG-C-LO and POWHEG-C-NLO are summarized in the present section. The numbers in parenthesis are the statistical errors on the last digit. The uncertainties are estimated from the scale dependence, as explained in the text.

Cuts	MCFM	POWHEG-NC	POWHEG-C-LO	POWHEG-C-NLO
Basic Photon	$23.47(1)^{+5\%}_{-8\%}$	$22.57(7)^{+10\%}_{-15\%}$	$23.52(7)^{+11\%}_{-16\%}$	$28.51(13)^{+4\%}_{-11\%}$
M_T cut	$5.839(1)^{+9\%}_{-9\%}$	$6.99(4)^{+14\%}_{-15\%}$	$7.11(4)^{+15\%}_{-16\%}$	$9.99(8)^{+14\%}_{-14\%}$
Lepton cuts	$2.227(1)^{+9\%}_{-10\%}$	$2.55(2)^{+14\%}_{-15\%}$	$2.67(2)^{+16\%}_{-17\%}$	$3.76(5)^{+17\%}_{-13\%}$

Table 4. The same as table 3 at $\sqrt{s} = 14$ TeV.

uncertainties arising from the scale dependence. We set the factorization and renormalization scales equal to $\mu_F = K_F \mu_0$ and $\mu_R = K_R \mu_0$, with $\mu_0 = M_W$,[13] and evaluate the cross sections for the following choices

$$(K_F, K_R) \in \left\{ \left(\frac{1}{2}, \frac{1}{2}\right), \left(\frac{1}{2}, 1\right), \left(\frac{1}{2}, 2\right), \left(1, \frac{1}{2}\right), (1, 1), (1, 2), \left(2, \frac{1}{2}\right), (2, 1), (2, 2) \right\} \quad (3.9)$$

that include variations of the two scales in the same and opposite directions. In fact, as motivated in ref. [19], varying the scales in opposite directions leads to a more reliable estimate of the theoretical uncertainty. The upper and lower values of the cross section that we quote are the upper and lower limits of the scale variation. The fragmentation scale is kept equal to M_W, as its variation does not lead to a significant change in the results, as discussed in ref. [19]. Concerning our results, which rely upon a dynamical treatment of the scales according to the MiNLO procedure, as described in section 2.4, the factorization scale variation is introduced both in the $W\gamma$ NLO and Wj LO/NLO dynamics (see eqs. (2.11), (2.14), (2.16) and (2.18)) according to the procedures described in refs. [35, 36], where a factor K_R is introduced that multiplies the MiNLO nodal scales, and a factor K_F is associated with the factorization scale.

In table 3 and table 4 the upper and lower extrema are obtained by calculating the cross section for both MCFM and POWHEG+MiNLO at $\{K_R = 1/2, K_F = 2\}$ and $\{K_R = 2, K_F = 1/2\}$, respectively, in agreement with the conclusion of ref. [19].

---

[13]We checked that no substantially different conclusions derive from the choice of a dynamical factorization/renormalization scale as central value in MCFM.

Before discussing the main aspects of these comparisons, let us remind, for clarity, the basic theoretical ingredients underlying the three POWHEG+MiNLO implementations realized in our work and considered in table 3 and table 4. As detailed in section 2.3.2, the three variants are characterized by the following main features:

- POWHEG-NC

  1. Accuracy: $\bar{B} = \bar{B}_{W\gamma} + B'_{Wj}$, with NLO QCD accuracy for $W\gamma$ production and LO accuracy for the Wj subprocess.

  2. Radiation dynamics: QCD radiation $R_{W\gamma;j}$ in $W\gamma$ production and QED radiation $R_{Wj;\gamma}$ in Wj contribution.

  3. SCALUP: as in the default POWHEG method for the $\bar{B}_{W\gamma}$ events and equal to the transverse momentum of the parton for the B_{Wj} contribution.

- POWHEG-C-LO

  1. $\bar{B} = \bar{B}_{W\gamma} + B'_{Wj}$, like for POWHEG-NC.

  2. Radiation dynamics: QCD radiation in $W\gamma$ production and QED+QCD emission in the Wj contribution.

  3. SCALUP: as in the default POWHEG, for both QCD radiation in the $\bar{B}_{W\gamma}$ events, and QED and QCD emission in the B'_{Wj} ones.

- POWHEG-C-NLO

  1. $\bar{B} = \bar{B}_{W\gamma} + \bar{B}_{Wj}$, with NLO QCD accuracy for both $W\gamma$ and Wj contributions.

  2. Radiation dynamics: the same as in POWHEG-C-LO.

  3. SCALUP: the same as in POWHEG-C-LO.

All the above ingredients are supplemented with the MiNLO procedure detailed in section 2.4 and by an interleaved QCD+QED simulation of multiple QCD and photon radiation.

As can be noticed from the results shown in table 3 and table 4, different considerations can be made, depending to a large extent on the assumed experimental setup.

First, it is evident that the theoretical uncertainties are pretty large, in particular at $\sqrt{s} = 14\,\mathrm{TeV}$, and this is a first hint of the importance of higher-order corrections to $W\gamma$ production at the LHC. In particular, it can be seen that the uncertainties associated to the POWHEG+MiNLO predictions are larger than those of MCFM, as a consequence of the quite different procedure used in the estimate of the theoretical uncertainty from the scale variations. In particular, our results receive an additional uncertainty driven by the evaluation of the Wj LO matrix elements and the $Wj(j)$ NLO cross section at relatively small transverse momenta.

In the presence of basic photon cuts only, the predictions of POWHEG-C-LO are in fairly good agreement with those of MCFM at both LHC energies. The cross sections obtained with the POWHEG-NC method are slightly lower, at the level of some percent, than those

obtained with POWHEG-C-LO. The same behavior is observed in the M_T or lepton cut selections, leading to the conclusion that the POWHEG-NC method is a good approximation of the POWHEG-C-LO one. On the other hand, the full NLO corrections to the Wj contribution, included in the POWHEG-C-NLO predictions, increases the cross section central values obtained with POWHEG-C-LO by about 15–20% in the basic photon selection, due to the presence of higher-order (beyond $O(\alpha_S)$) QCD contributions in our most accurate calculation.

In the presence of additional M_T or lepton cuts, different conclusions can be drawn. For such configurations, it is known that the NLO K-factors to the $W\gamma$ cross section at the LHC are quite large [19], approaching a factor of two. Under these conditions, the results obtained in terms of all our realizations are substantially different from the MCFM predictions. These discrepancies can be attributed to a number of reasons: the presence of PS effects and the modeling of the fragmentation contribution in all our algorithms, as well as the inclusion of the NLO corrections to the Wj subprocess in our POWHEG-C-NLO calculation.

The presence of large NLO corrections to the Wj process may be viewed as an indication that higher-order QCD contributions and, in particular, the yet unavailable NNLO corrections[14] may play a prominent rôle for a reliable theoretical interpretation of $W\gamma$ data at the LHC. On the other hand, we remind the reader that the Wj generated events may be view as an independent part of the production phase space, corresponding to the case when the emitted photon is softer than at least one jet in the event, while for $W\gamma$ generated events the photon is harder than all jets. Thus, it makes sense to include the NLO corrections to the Wj generated events, even if we do not attempt to include higher order corrections to the $W\gamma$ ones. Since these corrections are applied in different phase space regions, there is no reason to expect cancellations among them.

Regardless of the comparison to MCFM, it is also worth noting that the predictions provided by the algorithm POWHEG-NC and POWHEG-C-LO are in agreement at the some percent level both in the basic photon conditions and in the more exclusive M_T and lepton cut selections. While in the first algorithm, which mimics the approach of ref. [39], the QCD/QED interplay is modeled using an appropriate SCALUP choice for the QCD shower, in the second algorithm the radiation dynamics is described in a manner fully consistent with the default POWHEG method, using the correct Sudakov form factors for both photon and parton emissions from an underlying Wj Born configuration. The improved dynamical description of the radiation mechanism leads to some appreciable differences, even if we can conclude that the method proposed by D'Errico and Richardson in ref. [39] is already a realistic approximation of the our POWHEG-C-LO implementation.

To conclude this section, we show in table 5 the variation of a sample of our cross section results obtained by changing the parameters that define the photon isolation criteria. We restrict ourselves to the predictions of the POWHEG-C-LO implementation under lepton cuts conditions, as we checked that very similar conclusions hold for the other realizations and

---

[14]Preliminary results of a complete calculation of QCD corrections to the $W\gamma$ process at NNLO accuracy have been presented in ref. [25]. For a setup close to ATLAS analysis at 7 TeV, but using a smooth cone isolation requirement, the NNLO corrections amount to about +20%.

Photon isolation	POWHEG-C-LO $[\sqrt{s} = 7\,\text{TeV}]$	POWHEG-C-LO $[\sqrt{s} = 14\,\text{TeV}]$
$R_0 = 0.4,\ \epsilon_h = 0.4$	1.30(1)	2.64(2)
$R_0 = 0.4,\ \epsilon_h = 0.5$	1.31(1)	2.67(2)
$R_0 = 0.4,\ \epsilon_h = 0.6$	1.32(1)	2.70(2)
$\epsilon_h = 0.5,\ R_0 = 0.3$	1.34(1)	2.75(2)
$\epsilon_h = 0.5,\ R_0 = 0.5$	1.29(1)	2.60(2)

Table 5. Variation of the POWHEG+MiNLO predictions (POWHEG-C-LO implementation under lepton cuts conditions) for the cross section (in pb) of the $pp \to e^+\nu\gamma$ process at $\sqrt{s} = 7\,\text{TeV}$ and $\sqrt{s} = 14\,\text{TeV}$, respectively, due to a change of the photon isolation parameters ϵ_h and R_0.

experimental setup. We study the variation induced by a mild change of both the fraction ϵ_h of the transverse energy inside the cone and the cone size R_0. As can be seen, our results are stable against variations of ϵ_h and R_0 both at $\sqrt{s} = 7\,\text{TeV}$ and $\sqrt{s} = 14\,\text{TeV}$, as the cross section changes are of the order of a few percent. This suggests that the fragmentation contribution has a rather moderate impact on total prompt-photon production, in the presence of realistic photon isolation criteria.

3.2 Differential cross sections at $\sqrt{s} = 14\,\text{TeV}$: NLO vs. NLOPS predictions

In the studies of the $W\gamma$ process at the LHC, several distributions are considered in order to test SM predictions as well as to set limit on ATGCs and new vector resonance production [5, 8]. Here we limit ourselves to present our predictions for a particularly representative sample of differential cross sections at $\sqrt{s} = 14\,\text{TeV}$. Moreover, we focus on the results for the basic photon and lepton cuts only, as the considerations valid for the M_T cut conditions are similar to the latter case.

We show and comment the results obtained with all the three variants of our POWHEG implementations for the following distributions:

- the photon and lepton p_T;

- the transverse mass of the three-body system $e^+\nu\gamma$, i.e. $M_T^{\ell\nu\gamma}$;

- the photon-lepton rapidity difference $\Delta\eta(e^+\gamma)$;

and we compare our NLOPS simulations to the NLO MCFM predictions, including the MCFM theoretical uncertainties obtained from the scale dependence, estimated according to the method discussed for the total cross section (see eq. (3.9)).[15] The uncertainty bands that we quote are the envelope of the results obtained with the different scale choices. The results of these comparisons are shown in figure 4 and figure 5 for the basic photon and lepton cuts conditions, respectively. The MCFM uncertainties are shown in the lower panel of each plot, where the quantity Δ/MCFM is defined as $\Delta/\text{MCFM} = (d\sigma_{\text{PWG}} - d\sigma_{\text{MCFM}})/d\sigma_{\text{MCFM}}$, thus providing the relative deviation between our results and the NLO MCFM predictions.

---

[15]As for the comparisons at the level of integrated cross sections, we checked that the choice of a dynamical factorization/renormalization scale as central value in MCFM does not lead to substantially different conclusions.
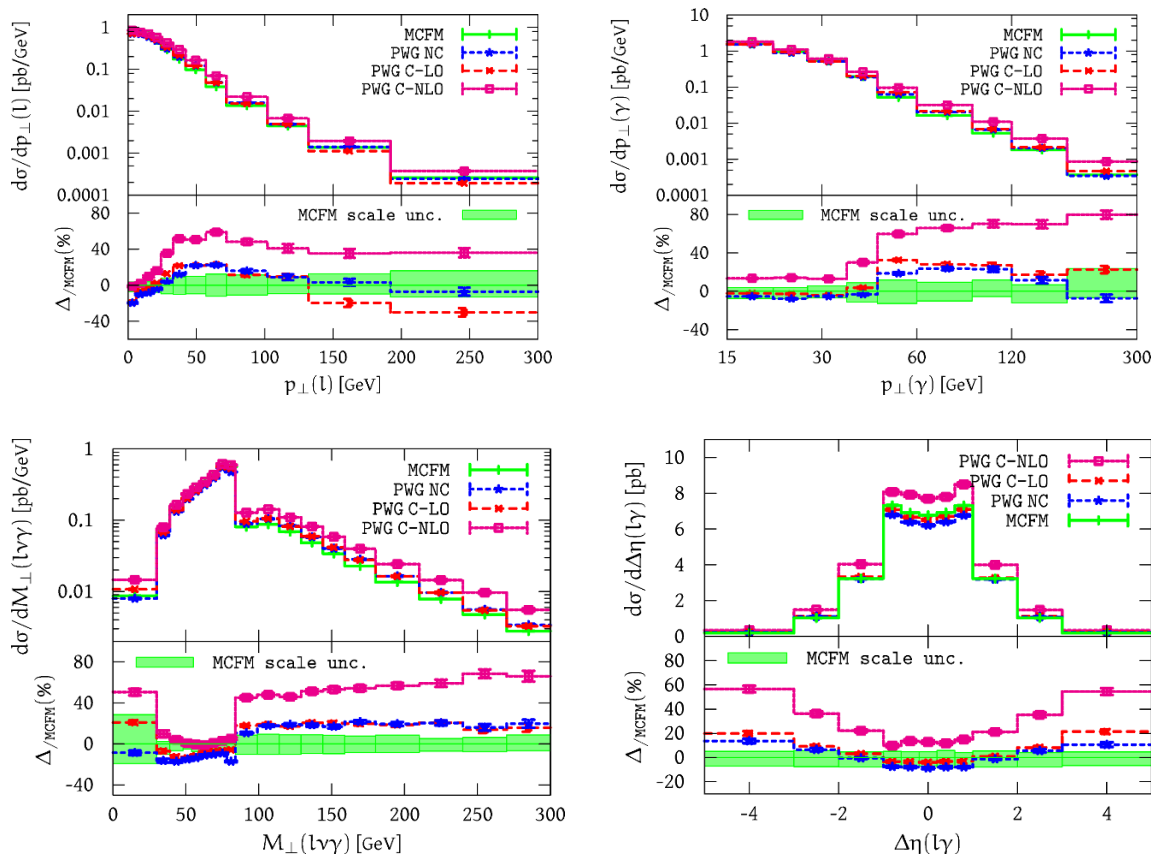
Figure 4. Comparison between the NLOPS results of the three `POWHEG`+MiNLO realizations and the `MCFM` NLO predictions for a number of distributions under basic photon cuts conditions. Upper plots: p_T^ℓ and p_T^γ distributions; lower plots: $M_T^{\ell\nu\gamma}$ and $\Delta\eta(\ell\gamma)$ distributions. The lower panels show $\Delta/\texttt{MCFM} = (d\sigma_{\texttt{PWG}} - d\sigma_{\texttt{MCFM}})/d\sigma_{\texttt{MCFM}}$, where the green band is the `MCFM` theoretical uncertainty obtained from the scale variation, as explained in the text.

For the basic photon setup, the shape of the differential cross sections predicted by MCFM and our NLOPS algorithms are rather different, in spite of the good agreement observed between MCFM and our results given by POWHEG-NC and POWHEG-C-LO at the level of integrated cross sections. This can be ascribed to the several different elements that are present in our calculation and are not included in the fixed order calculation. In particular, the region of small lepton momenta displays a marked difference in shape, since it is affected by our treatment of the separation between $W\gamma$ and Wj underlying Born processes, with the consequent use of the MiNLO procedure. On the other hand, it is apparent that the largest differences are observed with respect to the `POWHEG`-C-NLO scheme, due to the fact that in this scheme we include large QCD higher order corrections to the Wj process that are not at all present in the fixed order calculation.

From the lower panels of the plots shown in figure 4 it can be also seen that some large variations show up in the relative deviations of our predictions to those of `MCFM`. They are consequence of crossing points present in the shape of the distributions obtained in the two approaches. For example, in the $p_\perp^\gamma$ spectrum, the raise of the `POWHEG` result with respect
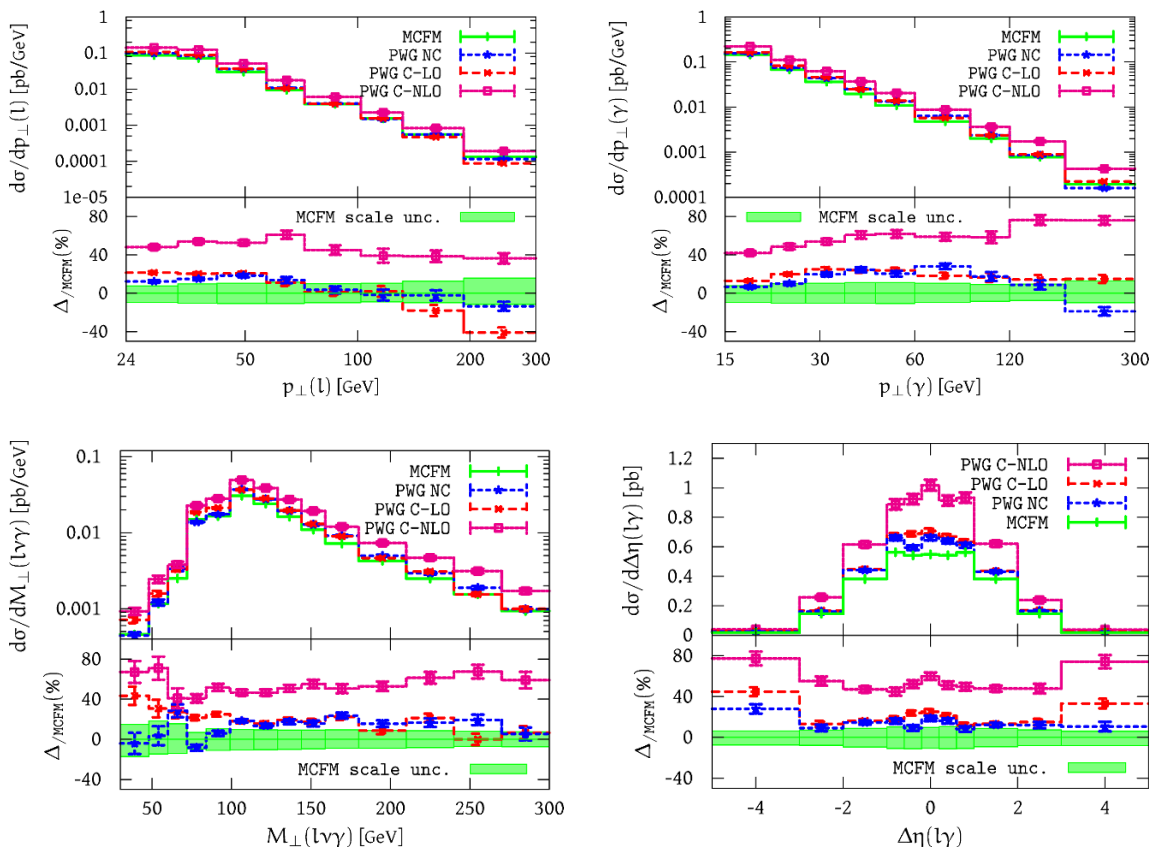
Figure 5. The same as figure 4 under lepton cuts conditions.

to the MCFM one around 50–60 GeV can be ascribed to the fact that photons from W decays are less likely above that value, and the two approaches have a very different treatment of the fragmentation contribution. Therefore, the main message of this comparison is that NLO and NLOPS calculations predict substantially different shapes for the differential cross sections of the $pp \to \ell\nu\gamma$ process when inclusive experimental conditions, i.e. without cuts on the lepton variables or on the transverse invariant masses, are considered.

A further conclusion that can be drawn from inspection of figure 4 is that the simulations obtained with the two algorithms POWHEG-NC and POWHEG-C-LO are in good agreement in the dominant regions of the distributions, thus explaining the agreement already noticed at the level of the integrated cross sections. On the other hand, the inclusion of the Wj contribution with normalization at NLO accuracy as in POWHEG-C-NLO gives rise to a relevant effect on the normalization of the distributions, outside the MCFM theoretical uncertainty band. The latter conclusion also holds for the distributions shown in figure 5 under lepton cuts conditions. However, in this case one can notice that the ratio of our predictions to those of MCFM is more uniform, as we have eliminated the differences that arise in the region of small lepton transverse momenta. Nevertheless, it can be seen that the predictions of all our POWHEG implementations are substantially different from those of MCFM at the normalization level.

Examples of NLOPS simulations of differential cross sections including an estimate of the theoretical uncertainty, are given in figure 6. We obtained the bands from the upper- and lower-bounding envelopes of the distributions, as already explained, but in terms of the variations of the dynamical factorization and renormalization scale described in section 3.1. We just show the results for the p_T^γ and $M_T^{\ell\nu\gamma}$ distributions in the basic photon (upper plots) and lepton cuts (lower plots) conditions, and we present the predictions of all the POWHEG+MiNLO implementations, i.e. POWHEG-NC (dashed lines) POWHEG-C-LO (orange band) and POWHEG-C-NLO (light orange band). The latter realizations share the same $O(\alpha_S^2) \, Wjj + \gamma_{PS}$ dynamics for the description of the real radiation mechanism, but differ in the LO(NLO) accuracy in the calculation of the Wj normalization. It can be seen that our estimate produces rather large theoretical uncertainties, as already remarked for the integrated cross section results. Moreover, the $Wj(j)$ NLO normalization contributions are not irrelevant at all in the whole p_T^γ and $M_T^{\ell\nu\gamma}$ range, especially in the extreme kinematical regions. As discussed earlier, this means that the corrections beyond NLO accuracy can play a relevant rôle for a reliable extraction of limits on ATGCs from the high tails of the p_T^γ differential cross section, especially in view of the experimental accuracy expected at the Run II of the LHC.

3.3 Comparisons to LHC data at $\sqrt{s} = 7\,\text{TeV}$

In this section we compare our predictions with all the data published by ATLAS collaboration for $W\gamma$ production at the LHC at $\sqrt{s} = 7\,\text{TeV}$ [5].[16] The lepton acceptance cuts and photon isolation criteria applied by ATLAS collaboration are the same as in eq. (3.4c), but jet identification requirements are also applied as follows

$$E_T^{\text{jet}} > 30 \text{ GeV}, \qquad |\eta_{\text{jet}}| < 4.4, \qquad \Delta R(e/\mu/\gamma, \text{jet}) > 0.3 \,. \tag{3.10}$$

Moreover, jets are defined according to an anti-k_T recombination algorithm, with separattion parameter $R_0 = 0.4$.[17] The data quoted by ATLAS refer to an inclusive ($N_{\text{jet}} \geq 0$) and exclusive ($N_{\text{jet}} = 0$) event selection. We present results for both conditions. For simplicity, the measured cross sections are compared with the predictions of the most accurate NLOPS simulations POWHEG-C-LO and POWHEG-C-NLO.

For the integrated cross section for the $\ell\nu\gamma$ process, $\ell = e^\pm$, we get the predictions

1. POWHEG-C-LO $\qquad \sigma(N_{\text{jet}} \geq 0)[\text{pb}] = 2.25^{+0.24}_{-0.24} \qquad \sigma(N_{\text{jet}} = 0)[\text{pb}] = 1.42^{+0.15}_{-0.15}$

2. POWHEG-C-NLO $\qquad \sigma(N_{\text{jet}} \geq 0)[\text{pb}] = 2.95^{+0.20}_{-0.38} \qquad \sigma(N_{\text{jet}} = 0)[\text{pb}] = 1.69^{+0.11}_{-0.22}$

where the theoretical uncertainties have been estimated from renormalization and factorization scale variations, according to the procedure described in section 3.1. These predictions must be compared to the ATLAS measured values [5]

$$\sigma_{\text{exp}}(N_{\text{jet}} \geq 0)[\text{pb}] = 2.74 \pm 0.05 \,(\text{stat}) \pm 0.32 \,(\text{syst}) \pm 0.14 \,(\text{lumi})$$
$$\sigma_{\text{exp}}(N_{\text{jet}} = 0)[\text{pb}] = 1.77 \pm 0.04 \,(\text{stat}) \pm 0.24 \,(\text{syst}) \pm 0.08 \,(\text{lumi}).$$

---

[16]We do not provide comparisons with CMS data, since they are quoted after corrections from MC simulations and just refer to three inclusive cross sections for $p_T^{\gamma,\text{min}} = 15, 60, 90\,\text{GeV}$ and a photon-lepton separation $\Delta R(\ell, \gamma) > 0.7$ [8].

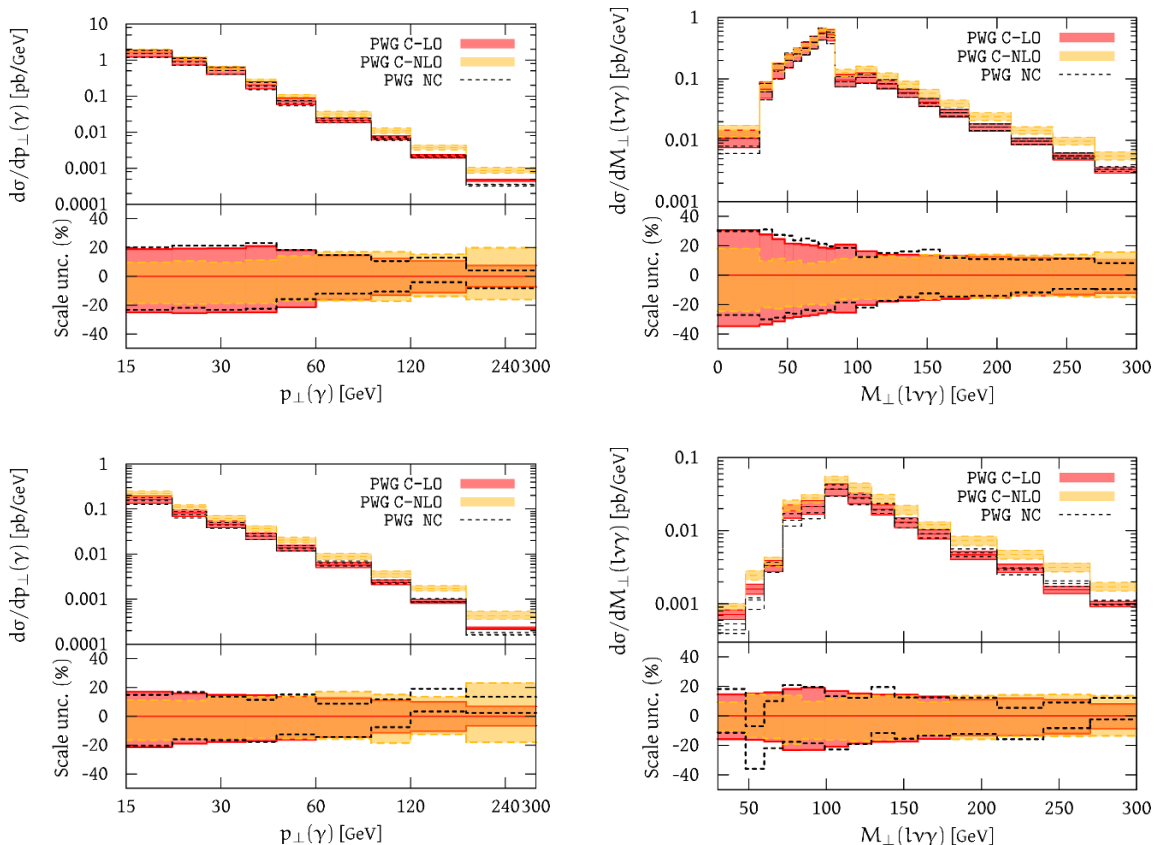[17]We implemented the jet algorithm using the FastJet code [82].

Figure 6. NLOPS simulations obtained with `POWHEG`-NC, `POWHEG`-C-LO and `POWHEG`-C-NLO for the p_T^γ and $M_T^{\ell\nu\gamma}$ distributions in the basic photon (upper plots) and lepton cuts (lower plots) conditions, respectively. The bands are an estimate of the theoretical uncertainty derived from the scale variation.

The `MCFM` results quoted by ATLAS for these configurations, after parton-to-particle level corrections, are

$$\sigma_{\text{MCFM}}(N_{\text{jet}} \ge 0)[\text{pb}] = 1.96 \pm 0.17 \qquad \sigma_{\text{MCFM}}(N_{\text{jet}} = 0)[\text{pb}] = 1.39 \pm 0.17$$

where the errors are an estimate of the theoretical systematic uncertainties, obtained by varying the PDFs, by changing the definition of photon isolation and by variation of the renormalization and factorizations scales from the nominal value $\mu_R = \mu_F = \sqrt{M_W^2 + p_T^{\gamma\,2}}$ up and down by a common factor of two.

It can be seen that our results, in particular the predictions provided by `POWHEG`-C-NLO, are in good agreement with the measured integrated cross sections, for both the inclusive and exclusive event selections.

The measured differential cross sections of the $pp \to \ell\nu\gamma$ process, obtained using combined electron and muon measurements, are shown in comparison to the NLOPS `POWHEG`+MiNLO simulations in figure 7 for the p_T^γ distribution in the inclusive and exclusive event selection, in figure 8 for normalized cross section as a function of $M_T^{\ell\nu\gamma}$ in the inclusive case (under the condition $p_T^\gamma > 40\,\text{GeV}$), and in figure 9 for the normalized cross

– 30 –
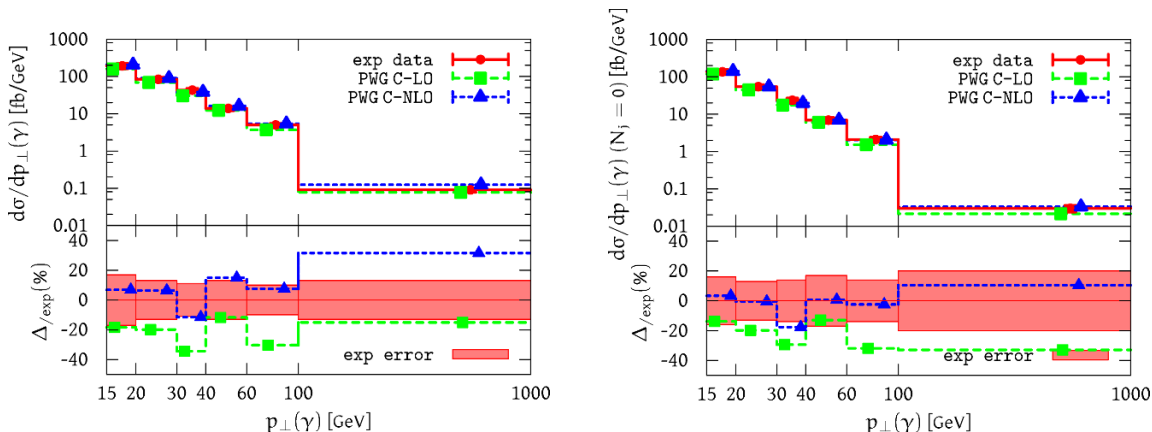
Figure 7. The p_T^γ differential cross sections of the $pp \rightarrow \ell\nu\gamma$ process measured by the ATLAS collaboration at $\sqrt{s} = 7\,\text{TeV}$ in the inclusive $N_{\text{jet}} \geq 0$ (left) and exclusive $N_{\text{jet}} = 0$ (right) event selections, in comparison to the NLOPS POWHEG+MiNLO predictions. The lower panels show $\Delta/\exp = (d\sigma_{\text{th.}} - d\sigma_{\text{exp.}})/d\sigma_{\text{exp.}}$, taking into account the total experimental uncertainty.

Figure 8. The normalized differential cross section of the $pp \rightarrow \ell\nu\gamma$ process measured by the ATLAS collaboration at $\sqrt{s} = 7\,\text{TeV}$ in the inclusive $N_{\text{jet}} \geq 0$ event selection as a function of $M_T^{\ell\nu\gamma}$ (for $p_T^\gamma > 40\,\text{GeV}$), in comparison to the NLOPS POWHEG+MiNLO predictions. The lower panels show $\Delta/\exp = (d\sigma_{\text{th.}} - d\sigma_{\text{exp.}})/d\sigma_{\text{exp.}}$, taking into account the total experimental uncertainty.

section as a function of the jet multiplicity with $p_T^\gamma > 15\,\text{GeV}$ and $p_T^\gamma > 60\,\text{GeV}$. In the lower panel of each plot we show the relative deviation $\Delta/\exp = (d\sigma_{\text{th.}} - d\sigma_{\text{exp.}})/d\sigma_{\text{exp.}}$ of the predictions to the data, including the total experimental uncertainty.

As can be seen, our theoretical results agree well with the data, as they reproduce the normalization and shape of the differential cross sections with good accuracy. In particular, while the predictions of POWHEG-C-LO are slightly lower than the data, the results of POWHEG-C-NLO, that includes the Wj dynamics with normalization at NLO accuracy, are in very good agreement with the measurements.
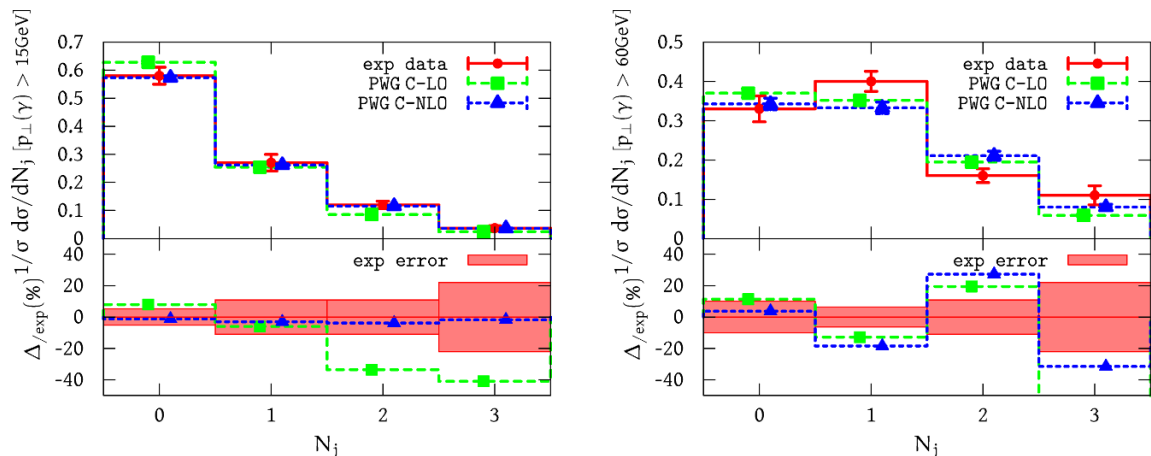
Figure 9. The differential cross section measurements of ATLAS collaboration at $\sqrt{s} = 7\,\text{TeV}$ as a function of the jet multiplicity for the $pp \to \ell\nu\gamma$ process, for $p_T^\gamma > 15\,\text{GeV}$ (left) and $p_T^\gamma > 60\,\text{GeV}$ (right), in comparison to the NLOPS POWHEG+MiNLO predictions. The lower panels show $\Delta/\text{exp} = (d\sigma_{\text{th.}} - d\sigma_{\text{exp.}})/d\sigma_{\text{exp.}}$, taking into account the total experimental uncertainty.

4 Conclusions

In this work we have presented an application of the POWHEG method, supplemented with the MiNLO procedure, to the theoretical treatment and simulation of the $W(\ell\nu)\gamma$ production process in hadronic collisions. We have shown how the method can be modified to cope with both the direct photon production and fragmentation contribution. To this end, we have used the matrix elements associated with the two different $W\gamma$ and Wj contributing processes and then showered and hadronized the generated events with a mixed QCD+QED parton shower, in order to provide a complete and fully exclusive description of the process under consideration. We have devised three different POWHEG+MiNLO descriptions of the $W\gamma$ process, characterized by increasing theoretical accuracy through the usage of QCD cross sections with LO/NLO accuracy matched to a PS. In particular, the method used in our most accurate simulations is a novel approach, that can be applied to any prompt-photon production process.

Our generator also includes the contribution of anomalous gauge couplings, in order to provide a complete tool for data analysis at the LHC. The code is available in the public repository of the POWHEG BOX [34] at the web site http://powhegbox.mib.infn.it.

In order to test the reliability of our calculation, we have compared our results with the predictions of the fixed-order MC program MCFM. In spite of the different treatment of the fragmentation mechanism, as well as of the presence in our approach of higher-order perturbative contributions, Sudakov and shower effects not included in MCFM, we observe an acceptable agreement with MCFM. However, this comparison also points out the relevance of higher-order perturbative and PS corrections for a reliable modeling of the differential cross sections of experimental interest, with a non-trivial dependence of those contributions on the considered event selection condition.

An alternative NLOPS-based method for the simulation of the interleaved QCD+QED emission off partons in a prompt-photon production processes was proposed in ref. [39].

We have also provided a variant of our generators that mimics its behaviour, and have found that this variant provides a good approximation of the QCD+QED competition mechanism.

A yet different approach to direct photon production was used, for example, in refs. [40, 41], to study $t\bar{t}\gamma$ and $t\bar{t}\gamma\gamma$ production. There, the photon emission is treated just like any other hard process in POWHEG, and the singularity associated to the photon are screened by introducing a technical cut, consisting in a smooth cone isolation applied to the photon. This is introduced using rather loose isolation parameters, assuming that they will not affect the cross section for realistic cuts. This approach is extremely simple, since it does not require either modifications to the POWHEG BOX machinery or mixed QED+QCD showers. In light of our present study, we consider this approach viable if the radiated photon is harder that the accompanying jets. If this is not the case, especially for a photon softer than two other jets in the event (i.e. when one jet is generated by the shower) the production probability does not reflect a consistent approximation to the real dynamics.

More importantly, we have compared our NLOPS simulations with the data published by ATLAS collaboration for the $pp \to \ell\nu\gamma$ process at the LHC at 7 TeV. We observe a good agreement between our predictions and the measured cross sections, for both the inclusive and exclusive event selections. In particular, both the normalization and shape of the measured differential cross section are reproduced remarkably well by our most accurate calculation.

The work presented here describes the first NLOPS simulation of the $W\gamma$ production process at hadron colliders. It contains several novel features in comparison to the existing theoretical literature about isolated photon hadroproduction and paves the way to the realization of future NNLOPS simulations of prompt photon production in a hadronic environment, thanks to the recent progress in this area [83–86] and the calculation of NNLO QCD corrections to specific processes involving isolated photons [24, 25, 87]. The approach can be easily adapted to deal with other relevant prompt-photon production reactions in hadronic collisions, such as $Z\gamma$ and $\gamma\gamma$ production. Moreover, the exclusive MC modeling of the fragmentation contribution presented in the paper provides a new way of performing interesting QCD studies of the measured photon fragmentation functions and of their typical theoretical parameterizations.

Acknowledgments

References

[1] ATLAS collaboration, *Observation of a new particle in the search for the Standard Model Higgs boson with the ATLAS detector at the LHC*, *Phys. Lett.* **B 716** (2012) 1 [arXiv:1207.7214] [INSPIRE].

[2] CMS collaboration, *Observation of a new boson at a mass of* 125 *GeV with the CMS experiment at the LHC*, *Phys. Lett.* **B 716** (2012) 30 [arXiv:1207.7235] [INSPIRE].

[3] M. Schott and J. Zhu, *Diboson production in proton-proton collisions at* $\sqrt{s} = 7\,TeV$, *Int. J. Mod. Phys.* **A 29** (2014) 1430053 [arXiv:1406.7731] [INSPIRE].

[4] ATLAS collaboration, *Search for new resonances in* $W\gamma$ *and* $Z\gamma$ *final states in pp collisions at* $\sqrt{s} = 8\,TeV$ *with the ATLAS detector*, *Phys. Lett.* **B 738** (2014) 428 [arXiv:1407.8150] [INSPIRE].

[5] ATLAS collaboration, *Measurements of* $W\gamma$ *and* $Z\gamma$ *production in pp collisions at* $\sqrt{s} = 7\,TeV$ *with the ATLAS detector at the LHC*, *Phys. Rev.* **D 87** (2013) 112003 [arXiv:1302.1283] [INSPIRE].

[6] ATLAS collaboration, *Measurement of* $W\gamma$ *and* $Z\gamma$ *production cross sections in pp collisions at* $\sqrt{s} = 7\,TeV$ *and limits on anomalous triple gauge couplings with the ATLAS detector*, *Phys. Lett.* **B 717** (2012) 49 [arXiv:1205.2531] [INSPIRE].

[7] ATLAS collaboration, *Measurement of* $W\gamma$ *and* $Z\gamma$ *production in proton-proton collisions at* $\sqrt{s} = 7\,TeV$ *with the ATLAS Detector*, *JHEP* **09** (2011) 072 [arXiv:1106.1592] [INSPIRE].

[8] CMS collaboration, *Measurement of the* $W\gamma$ *and* $Z\gamma$ *inclusive cross sections in pp collisions at* $\sqrt{s} = 7\,TeV$ *and limits on anomalous triple gauge boson couplings*, *Phys. Rev.* **D 89** (2014) 092005 [arXiv:1308.6832] [INSPIRE].

[9] CMS collaboration, *Measurement of the production cross section for* $Z\gamma \to \nu\bar{\nu}\gamma$ *in pp collisions at* $\sqrt{s} = 7\,TeV$ *and limits on* $ZZ\gamma$ *and* $Z\gamma\gamma$ *triple gauge boson couplings*, *JHEP* **10** (2013) 164 [arXiv:1309.1117] [INSPIRE].

[10] CMS collaboration, *Measurement of* $W\gamma$ *and* $Z\gamma$ *production in pp collisions at* $\sqrt{s} = 7\,TeV$, *Phys. Lett.* **B 701** (2011) 535 [arXiv:1105.2758] [INSPIRE].

[11] CDF collaboration, T. Aaltonen et al., *Limits on Anomalous Trilinear Gauge Couplings in* $Z\gamma$ *Events from* $p\bar{p}$ *Collisions at* $\sqrt{s} = 1.96\,TeV$, *Phys. Rev. Lett.* **107** (2011) 051802 [arXiv:1103.2990] [INSPIRE].

[12] D0 collaboration, V.M. Abazov et al., $Z\gamma$ *production and limits on anomalous* $ZZ\gamma$ *and* $Z\gamma\gamma$ *couplings in* $p\bar{p}$ *collisions at* $\sqrt{s} = 1.96\,TeV$, *Phys. Rev.* **D 85** (2012) 052001 [arXiv:1111.3684] [INSPIRE].

[13] D0 collaboration, V.M. Abazov et al., $W\gamma$ *production and limits on anomalous* $WW\gamma$ *couplings in* $p\bar{p}$ *collisions*, *Phys. Rev. Lett.* **107** (2011) 241803 [arXiv:1109.4432] [INSPIRE].

[14] ALEPH, DELPHI, L3, OPAL collaborations, LEP ELECTROWEAK Working Group, J. Alcaraz et al., *A Combination of preliminary electroweak measurements and constraints on the standard model*, hep-ex/0612034 [INSPIRE].

[15] M.L. Mangano, M. Moretti, F. Piccinini, R. Pittau and A.D. Polosa, *ALPGEN, a generator for hard multiparton processes in hadronic collisions*, *JHEP* **07** (2003) 001 [hep-ph/0206293] [INSPIRE].

[16] J. Alwall, M. Herquet, F. Maltoni, O. Mattelaer and T. Stelzer, *MadGraph 5: Going Beyond*, *JHEP* **06** (2011) 128 [arXiv:1106.0522] [INSPIRE].

[17] T. Gleisberg, S. Höche, F. Krauss, A. Schalicke, S. Schumann and J.-C. Winter, *SHERPA 1. α: A Proof of concept version*, *JHEP* **02** (2004) 056 [hep-ph/0311263] [INSPIRE].

[18] J.M. Campbell and R.K. Ellis, *MCFM for the Tevatron and the LHC*, *Nucl. Phys. Proc. Suppl.* **205-206** (2010) 10 [arXiv:1007.3492] [INSPIRE].

[19] J.M. Campbell, R.K. Ellis and C. Williams, *Vector boson pair production at the LHC*, *JHEP* **07** (2011) 018 [arXiv:1105.0020] [INSPIRE].

[20] J. Ohnemus, *Order-α_s calculations of hadronic $W^{\pm}\gamma$ and $Z\gamma$ production*, *Phys. Rev.* **D 47** (1993) 940 [INSPIRE].

[21] U. Baur, T. Han and J. Ohnemus, *QCD corrections to hadronic $W\gamma$ production with nonstandard $WW\gamma$ couplings*, *Phys. Rev.* **D 48** (1993) 5140 [hep-ph/9305314] [INSPIRE].

[22] U. Baur, T. Han and J. Ohnemus, *QCD corrections and anomalous couplings in $Z\gamma$ production at hadron colliders*, *Phys. Rev.* **D 57** (1998) 2823 [hep-ph/9710416] [INSPIRE].

[23] D. De Florian and A. Signer, *$W\gamma$ and $Z\gamma$ production at hadron colliders*, *Eur. Phys. J.* **C 16** (2000) 105 [hep-ph/0002138] [INSPIRE].

[24] M. Grazzini, S. Kallweit, D. Rathlev and A. Torre, *$Z\gamma$ production at hadron colliders in NNLO QCD*, *Phys. Lett.* **B 731** (2014) 204 [arXiv:1309.7000] [INSPIRE].

[25] M. Grazzini, *Vector-boson pair production at NNLO*, PoS(LL2014)027 [arXiv:1407.1618] [INSPIRE].

[26] F. Campanario, C. Englert, M. Spannowsky and D. Zeppenfeld, *NLO-QCD corrections to $W\gamma j$ production*, *Europhys. Lett.* **88** (2009) 11001 [arXiv:0908.1638] [INSPIRE].

[27] F. Campanario, N. Kaiser and D. Zeppenfeld, *$W\gamma$ production in vector boson fusion at NLO in QCD*, *Phys. Rev.* **D 89** (2014) 014009 [arXiv:1309.7259] [INSPIRE].

[28] F. Campanario, M. Kerner, L.D. Ninh and D. Zeppenfeld, *Next-to-leading order QCD corrections to $W\gamma$ production in association with two jets*, *Eur. Phys. J.* **C 74** (2014) 2882 [arXiv:1402.0505] [INSPIRE].

[29] F. Campanario, M. Kerner, L.D. Ninh and D. Zeppenfeld, *$Z\gamma$ production in association with two jets at next-to-leading order QCD*, *Eur. Phys. J.* **C 74** (2014) 3085 [arXiv:1407.7857] [INSPIRE].

[30] E. Accomando, A. Denner and C. Meier, *Electroweak corrections to $W\gamma$ and $Z\gamma$ production at the LHC*, *Eur. Phys. J.* **C 47** (2006) 125 [hep-ph/0509234] [INSPIRE].

[31] W. Hollik and C. Meier, *Electroweak corrections to γZ production at hadron colliders*, *Phys. Lett.* **B 590** (2004) 69 [hep-ph/0402281] [INSPIRE].

[32] P. Nason, *A New method for combining NLO QCD with shower Monte Carlo algorithms*, *JHEP* **11** (2004) 040 [hep-ph/0409146] [INSPIRE].

[33] S. Frixione, P. Nason and C. Oleari, *Matching NLO QCD computations with Parton Shower simulations: the POWHEG method*, *JHEP* **11** (2007) 070 [arXiv:0709.2092] [INSPIRE].

[34] S. Alioli, P. Nason, C. Oleari and E. Re, *A general framework for implementing NLO calculations in shower Monte Carlo programs: the POWHEG BOX*, *JHEP* **06** (2010) 043 [arXiv:1002.2581] [INSPIRE].

[35] K. Hamilton, P. Nason, C. Oleari and G. Zanderighi, *Merging H/W/Z + 0 and 1 jet at NLO with no merging scale: a path to parton shower + NNLO matching*, *JHEP* **05** (2013) 082 [arXiv:1212.4504] [INSPIRE].

[36] K. Hamilton, P. Nason and G. Zanderighi, *MINLO: Multi-Scale Improved NLO*, *JHEP* **10** (2012) 155 [arXiv:1206.3572] [INSPIRE].

[37] PARTICLE DATA GROUP collaboration, K. Olive et al., *Review of Particle Physics*, *Chin. Phys.* **C 38** (2014) 090001 [INSPIRE].

[38] S. Höche, S. Schumann and F. Siegert, *Hard photon production and matrix-element parton-shower merging*, *Phys. Rev.* **D 81** (2010) 034026 [arXiv:0912.3501] [INSPIRE].

[39] L. D'Errico and P. Richardson, *Next-to-Leading-Order Monte Carlo Simulation of Diphoton Production in Hadronic Collisions*, *JHEP* **02** (2012) 130 [arXiv:1106.3939] [INSPIRE].

[40] A. Kardos and Z. Trócsányi, *Hadroproduction of t anti-t pair in association with an isolated photon at NLO accuracy matched with parton shower*, arXiv:1406.2324 [INSPIRE].

[41] A. Kardos and Z. Trócsányi, *Hadroproduction of t anti-t pair with two isolated photons with PowHel*, arXiv:1408.0278 [INSPIRE].

[42] J.A.M. Vermaseren, *New features of FORM*, math-ph/0010025 [INSPIRE].

[43] R.W. Brown, D. Sahdev and K.O. Mikaelian, $W^\pm Z^0$ *and* $W^\pm \gamma$ *Pair Production νe, pp and $\bar{p}p$ Collisions*, *Phys. Rev.* **D 20** (1979) 1164 [INSPIRE].

[44] K.O. Mikaelian, M.A. Samuel and D. Sahdev, *The Magnetic Moment of Weak Bosons Produced in pp and p$\bar{p}$ Collisions*, *Phys. Rev. Lett.* **43** (1979) 746 [INSPIRE].

[45] D0 collaboration, V.M. Abazov et al., *First study of the radiation-amplitude zero in $W\gamma$ production and limits on anomalous $WW\gamma$ couplings at $\sqrt{s} = 1.96$ TeV*, *Phys. Rev. Lett.* **100** (2008) 241805 [arXiv:0803.0030] [INSPIRE].

[46] K.J.F. Gaemers and G.J. Gounaris, *Polarization Amplitudes for $e^+e^- \to W^+W^-$ and $e^+e^- \to ZZ$*, *Z. Phys.* **C 1** (1979) 259 [INSPIRE].

[47] K. Hagiwara, R.D. Peccei, D. Zeppenfeld and K. Hikasa, *Probing the Weak Boson Sector in $e^+e^- \to W^+W^-$*, *Nucl. Phys.* **B 282** (1987) 253 [INSPIRE].

[48] U. Baur and D. Zeppenfeld, *Probing the $WW\gamma$ Vertex at Future Hadron Colliders*, *Nucl. Phys.* **B 308** (1988) 127 [INSPIRE].

[49] U. Baur and E.L. Berger, *Probing the $WW\gamma$ Vertex at the Tevatron Collider*, *Phys. Rev.* **D 41** (1990) 1476 [INSPIRE].

[50] F.A. Berends and A.I. van Sighem, *Anomalous four fermion processes in electron-positron collisions*, *Nucl. Phys.* **B 454** (1995) 467 [hep-ph/9506391] [INSPIRE].

[51] C. Degrande et al., *Effective Field Theory: A Modern Approach to Anomalous Couplings*, *Annals Phys.* **335** (2013) 21 [arXiv:1205.4231] [INSPIRE].

[52] G. Passarino and M.J.G. Veltman, *One Loop Corrections for e^+e^- Annihilation Into $\mu^+\mu^-$ in the Weinberg Model*, *Nucl. Phys.* **B 160** (1979) 151 [INSPIRE].

[53] Z. Kunszt, A. Signer and Z. Trócsányi, *One loop helicity amplitudes for all* $2 \to 2$ *processes in QCD and* $N = 1$ *supersymmetric Yang-Mills theory*, *Nucl. Phys.* **B 411** (1994) 397 [hep-ph/9305239] [INSPIRE].

[54] T. Gehrmann, N. Greiner and G. Heinrich, *Photon isolation effects at NLO in* $\gamma\gamma$ + *jet final states in hadronic collisions*, *JHEP* **06** (2013) 058 [*Erratum ibid.* **1406** (2014) 076] [arXiv:1303.0824] [INSPIRE].

[55] H.B. Hartanto and L. Reina, *Hard-photon production with b jets at hadron colliders*, *Phys. Rev.* **D 89** (2014) 074001 [arXiv:1312.2384] [INSPIRE].

[56] J.M. Campbell and C. Williams, *Triphoton production at hadron colliders*, *Phys. Rev.* **D 89** (2014) 113001 [arXiv:1403.2641] [INSPIRE].

[57] T. Binoth, J.-P. Guillet, E. Pilon and M. Werlen, *A Full next-to-leading order study of direct photon pair production in hadronic collisions*, *Eur. Phys. J.* **C 16** (2000) 311 [hep-ph/9911340] [INSPIRE].

[58] S. Catani, M. Fontannaz, J.-P. Guille and E. Pilon, *Cross section of isolated prompt photons in hadron-hadron collisions*, *JHEP* **05** (2002) 028 [hep-ph/0204023] [INSPIRE].

[59] P. Aurenche, M. Fontannaz, J.-P. Guillet, E. Pilon and M. Werlen, *A New critical study of photon production in hadronic collisions*, *Phys. Rev.* **D 73** (2006) 094007 [hep-ph/0602133] [INSPIRE].

[60] C.H. Llewellyn Smith, *QCD Predictions for Processes Involving Real Photons*, *Phys. Lett.* **B 79** (1978) 83 [INSPIRE].

[61] L. Bourhis, M. Fontannaz and J.-P. Guille, *Quarks and gluon fragmentation functions into photons*, *Eur. Phys. J.* **C 2** (1998) 529 [hep-ph/9704447] [INSPIRE].

[62] H. Baer, J. Ohnemus and J.F. Owens, *A Next-to-leading Logarithm Calculation of Direct Photon Production*, *Phys. Rev.* **D 42** (1990) 61 [INSPIRE].

[63] P. Aurenche, R. Baier and M. Fontannaz, *Prompt Photon Production at Colliders*, *Phys. Rev.* **D 42** (1990) 1440 [INSPIRE].

[64] E.W.N. Glover and A.G. Morgan, *Measuring the photon fragmentation function at LEP*, *Z. Phys.* **C 62** (1994) 311 [INSPIRE].

[65] S. Frixione, *Isolated photons in perturbative QCD*, *Phys. Lett.* **B 429** (1998) 369 [hep-ph/9801442] [INSPIRE].

[66] S. Frixione, Z. Kunszt and A. Signer, *Three jet cross-sections to next-to-leading order*, *Nucl. Phys.* **B 467** (1996) 399 [hep-ph/9512328] [INSPIRE].

[67] L. Barzè, G. Montagna, P. Nason, O. Nicrosini and F. Piccinini, *Implementation of electroweak corrections in the POWHEG BOX: single W production*, *JHEP* **04** (2012) 037 [arXiv:1202.0465] [INSPIRE].

[68] L. Barzè, G. Montagna, P. Nason, O. Nicrosini, F. Piccinini and A. Vicini, *Neutral current Drell-Yan with combined QCD and electroweak corrections in the POWHEG BOX*, *Eur. Phys. J.* **C 73** (2013) 2474 [arXiv:1302.4606] [INSPIRE].

[69] M. Bähr et al., *HERWIG++ Physics and Manual*, *Eur. Phys. J.* **C 58** (2008) 639 [arXiv:0803.0883] [INSPIRE].

[70] T. Sjöstrand, S. Mrenna and P.Z. Skands, *PYTHIA 6.4 Physics and Manual*, *JHEP* **05** (2006) 026 [hep-ph/0603175] [INSPIRE].

[71] T. Sjöstrand, S. Mrenna and P.Z. Skands, *A Brief Introduction to PYTHIA 8.1*, *Comput. Phys. Commun.* **178** (2008) 852 [arXiv:0710.3820] [InSPIRE].

[72] S. Alioli, P. Nason, C. Oleari and E. Re, *Vector boson plus one jet production in POWHEG*, *JHEP* **01** (2011) 095 [arXiv:1009.5594] [InSPIRE].

[73] S. Catani, F. Krauss, R. Kuhn and B.R. Webber, *QCD matrix elements + parton showers*, *JHEP* **11** (2001) 063 [hep-ph/0109231] [InSPIRE].

[74] L. Lönnblad, *Correcting the color dipole cascade model with fixed order matrix elements*, *JHEP* **05** (2002) 046 [hep-ph/0112284] [InSPIRE].

[75] F. Krauss, *Matrix elements and parton showers in hadronic interactions*, *JHEP* **08** (2002) 015 [hep-ph/0205283] [InSPIRE].

[76] S. Mrenna and P. Richardson, *Matching matrix elements and parton showers with HERWIG and PYTHIA*, *JHEP* **05** (2004) 040 [hep-ph/0312274] [InSPIRE].

[77] J.M. Campbell, R.K. Ellis, P. Nason and G. Zanderighi, *W and Z bosons in association with two jets using the POWHEG method*, *JHEP* **08** (2013) 005 [arXiv:1303.5447] [InSPIRE].

[78] G. Luisoni, P. Nason, C. Oleari and F. Tramontano, $HW^{\pm}/HZ + 0$ *and 1 jet at NLO with the POWHEG BOX interfaced to GoSam and their merging within MiNLO*, *JHEP* **10** (2013) 083 [arXiv:1306.2542] [InSPIRE].

[79] H.-L. Lai et al., *New parton distributions for collider physics*, *Phys. Rev.* **D 82** (2010) 074024 [arXiv:1007.2241] [InSPIRE].

[80] A.D. Martin, W.J. Stirling, R.S. Thorne and G. Watt, *Parton distributions for the LHC*, *Eur. Phys. J.* **C 63** (2009) 189 [arXiv:0901.0002] [InSPIRE].

[81] R.D. Ball et al., *A first unbiased global NLO determination of parton distributions and their uncertainties*, *Nucl. Phys.* **B 838** (2010) 136 [arXiv:1002.4407] [InSPIRE].

[82] M. Cacciari, G.P. Salam and G. Soyez, *FastJet User Manual*, *Eur. Phys. J.* **C 72** (2012) 1896 [arXiv:1111.6097] [InSPIRE].

[83] K. Hamilton, P. Nason, E. Re and G. Zanderighi, *NNLOPS simulation of Higgs boson production*, *JHEP* **10** (2013) 222 [arXiv:1309.0017] [InSPIRE].

[84] S. Höche, Y. Li and S. Prestel, *Drell-Yan lepton pair production at NNLO QCD with parton showers*, arXiv:1405.3607 [InSPIRE].

[85] A. Karlberg, E. Re and G. Zanderighi, *NNLOPS accurate Drell-Yan production*, *JHEP* **09** (2014) 134 [arXiv:1407.2940] [InSPIRE].

[86] S. Höche, Y. Li and S. Prestel, *Higgs-boson production through gluon fusion at NNLO QCD with parton showers*, arXiv:1407.3773 [InSPIRE].

[87] S. Catani, L. Cieri, D. de Florian, G. Ferrera and M. Grazzini, *Diphoton production at hadron colliders: a fully-differential QCD calculation at NNLO*, *Phys. Rev. Lett.* **108** (2012) 072001 [arXiv:1110.2375] [InSPIRE].